AD-757 103

ARCTIC SITE SURVEY, PART I

T. S. Chow

Aerophysics Research Corporation

Prepared for:

Office of Naval Research
Advanced Research Projects Agency

15 March 1973

ARPA Order Number
1779/dtd. 11-16-71

Program Code Number
2N10

Name of Contractor
Aerophysics Research Corporation

Effective Date of Contract
April 1, 1972

Contract Expiration Date
December 31, 1972

Amount of Contract
$ 63638.00

Contract Number
N00014-72-C-0335

Principal Investigator & Ph #
T. S. Chow (206) 454-6927

Scientific Officer
Director, Arctic Program
Earth Sciences Division
Office of Naval Research
Dept. of the Navy
800 N. Quincy Street
Arlington, Virginia 22217

Short Title of Work
ARCTIC SITE SURVEY
(Part I)

15 March 1973

Sponsored by
Advanced Research Projects Agency
ARPA Order No.
1779/dtd. 11-16-71

TABLE OF CONTENTS

1. SUMMARY

The principal objectives of this work are:

(1) to investigate ray theory, normal mode or any newly-developed method by comparing the computed results with field measured data for predicting underwater sound propagation loss in the Arctic, and

(2) to apply appropriate techniques to evaluate acoustic intensity and transmission loss at promising locations from a number of sound sources in the Arctic.

Because of the limited time available for completion of the project, efforts to fulfil both objectives had to be pursued at the same time. Thus while a program of research using direct integration (FFP, Section 5) was being carried out at Lamont-Doherty Geological Observatory, concurrently a ray tracing program geared specifically for the calculation of acoustic intensities in the Arctic was being implemented at Aerophysics Research Corporation.

Details of the direct integration method are given in a separate report (Reference 5, Section 5). Comparisons of results calculated by ray theory and by direct integration are illustrated on page 89.

The Arctic Ocean bottom is graphically illustrated on pages 61-65 by plotting the various depth contours. These and other considerations have led to the choice of a number of sound sources and receivers, which are partitioned into five groups roughly in accordance with the bottom topography. The location of the sources and receivers is tabulated and indicated in the contour maps on pages 67-76.

Comparisons of field measured loss-range curves with calculated results by ray theory are shown on pages 77-88. The complete computer output of acoustic intensities and transmission loss is presented in Part II of the report. It is indeed gratifying to note that on the whole the computed results agree well with field data.

As follow up work in the future the following suggestions will be made.

(1) Several refinements can be experimented and explored in the ray tracing program. Correction for acoustic intensity for regions close to the caustic zones should be re-examined. Also the bottom reflection loss calculations can be reformulated by utilizing more information of the bottom topography. Similarly the direct integration method can be developed further to take into consideration a varying bottom.

(2) Site survey (propagation loss calculations) will be carried out at various frequencies in the band 10 to 500 hz. Specifically computations are to be performed by both ray theory and direct integration as cross-check at 10, 15, 20, 30, 50, 60, 80, 100, 150, 200, 250, 300, 400 and 500 hz.

(3) From the results of (2) the detection ranges for typical surface and underwater sources will be estimated from the sonar equation. Detection systems which appear feasible for use in the Arctic will be considered, viz., various types of hydrophone arrays, signal processing, data display and data gathering.

The fact that now rapid and efficient prediction can be made on the underwater sound transmission loss indeed paves the way for future exploration and research in the Arctic Ocean area.

2. THEORETICAL DEVELOPMENTS

2.1 ENERGY ALONG A RAY PATH

Consider two-dimensional ray propagation in the (x,y) plane with sound velocity $c = c(x,y)$

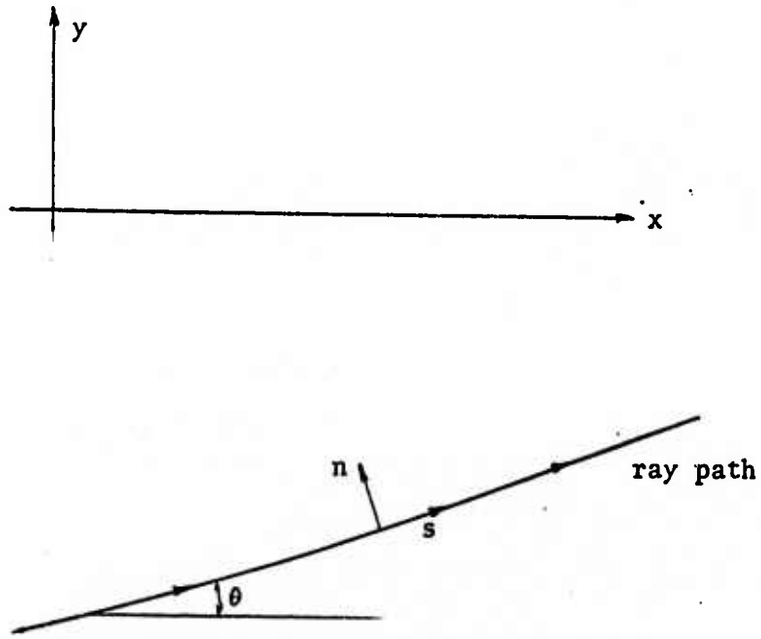

Fig. 1

Let s be the distance measured along a ray and let n denote the local orthogonal direction as shown. If θ is the slope angle of the ray, the $(\vec{s}, \vec{n})$ vectors are obtained by rotating the $(\vec{x}, \vec{y})$ vectors counterclockwise through θ.

The curvature 1/R is given by

$$\frac{1}{R} = \frac{d\theta}{ds} \tag{1}$$

Since the ray equations read

$$\begin{aligned} c\,\frac{d^2x}{ds^2} &= \left(c_x \frac{dx}{ds} + c_y \frac{dy}{ds}\right)\frac{dx}{ds} - c_x \\ c\,\frac{d^2y}{ds^2} &= \left(c_x \frac{dx}{ds} + c_y \frac{dy}{ds}\right)\frac{dy}{ds} - c_y \end{aligned} \tag{2}$$

It follows easily that

$$c\,\frac{d\theta}{ds} = c_x \sin\theta - c_y \cos\theta = -\frac{\partial c}{\partial n}$$

so that

$$\frac{1}{R} = \frac{\partial}{\partial n}(\ell n\ c) \qquad (3)$$

The rays are orthogonal to surfaces of constant phase; for brevity, such surfaces will be termed *wave fronts*. Denote the local curvature of a wave front by $(1/R_w)$; taken as positive η the rays are diverging. The immediate purpose is to compute $d/ds(1/R_w)$.

For convenience, introduce an orthogonal curvilinear coordinate system with ξ constant on a ray and η constant on a wave front.

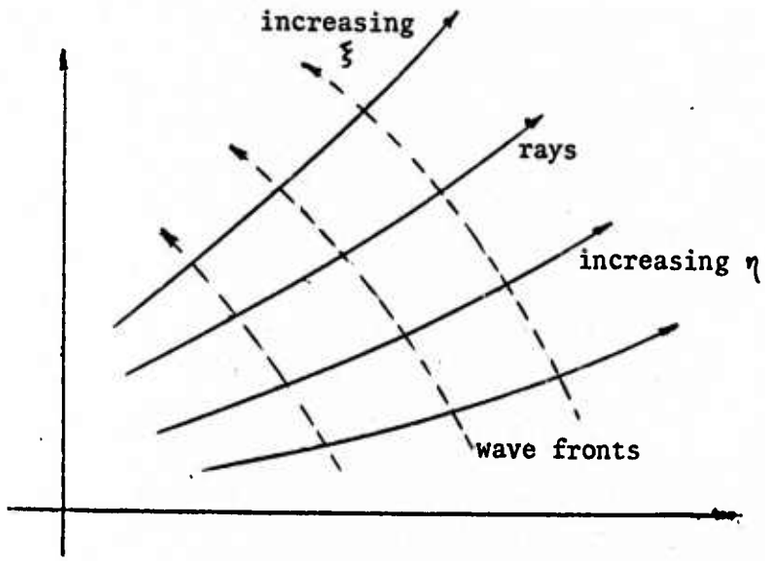

Fig. 2

Clearly,

$$\tan\theta = \frac{y_\eta}{x_\eta} = -\frac{x_\xi}{y_\xi} \qquad (4)$$

and

$$\frac{1}{R} = \frac{\theta_\eta}{x_\eta}\cos\theta\ ,\ \frac{1}{R_w} = \frac{\theta_\xi}{y_\xi}\cos\theta \qquad (5)$$

Thus,

$$\frac{d}{ds}\left(\frac{1}{R_w}\right) = \left(\frac{\theta_\xi}{y_\xi}\cos\theta\right)_\eta \frac{\cos\theta}{x_\eta}$$

$$= \frac{\cos\theta}{x_\eta y_\xi}\left[\theta_{\xi\eta}\cos\theta - \frac{\theta_\xi y_{\xi\eta}\cos\theta}{y_\xi} - \theta_\xi\theta_\eta\sin\theta\right] \qquad (6)$$

Similarly,

$$\frac{d}{dn}\left(\frac{1}{R}\right) = \frac{\cos\theta}{x_\eta y_\xi}\left[\theta_{\xi\eta}\cos\theta - \frac{\theta_\eta x_{\xi\eta}\cos\theta}{x_\eta} - \theta_\xi\theta_\eta\sin\theta\right] \qquad (7)$$

combining, we obtain

$$\frac{d}{ds}\left(\frac{1}{R_w}\right) = \frac{d}{dn}\left(\frac{1}{R}\right) + \frac{\cos\theta}{x_\eta y_\xi}\left(\frac{x_{\xi\eta}}{R} - \frac{y_{\xi\eta}}{R_w}\right) \qquad (8)$$

Next, differentiate the first of Equations (4) with respect to ξ and the second with respect to η ; then solve the resulting equations for $y_{\xi\eta}$ and $x_{\xi\eta}$ to obtain (with the help of Equations (5))

$$y_{\xi\eta} = \frac{x_\eta y_\xi}{\cos\theta}\left(\frac{1}{R_w} - \frac{\tan\theta}{R}\right)$$

$$x_{\xi\eta} = \frac{x_\eta y_\xi}{\cos\theta}\left(-\frac{1}{R} - \frac{\tan\theta}{R_w}\right) \qquad (9)$$

Substitution into Equation (8) now gives the desired result:

$$\frac{d}{ds}\left(\frac{1}{R_w}\right) = \frac{d}{dn}\left(\frac{1}{R}\right) - \frac{1}{R^2} - \frac{1}{R_w^2} \qquad (10)$$

To obtain a convenient formula for d/dn(1/R), we observe that Equation (3) yields the following.

$$\frac{d}{dn}\left(\frac{1}{R}\right) = \frac{d}{dn}[(\ell n\ c)_x \sin\theta - (\ell n\ c)_y \cos\theta]$$

$$= [(\ell n\ c)_x \cos\theta + (\ell n\ c)_y \sin\theta]\ \frac{d\theta}{dn}$$

$$- [(\ell n\ c)_{xx} \sin^2\theta - 2(\ell n\ c)_{xy} \sin\theta \cos\theta + (\ell n\ c)_{yy} \cos^2\theta]$$

$$= \frac{1}{R_w}\left[\frac{d}{ds}(\ell n\ c)\right] - \frac{d^2}{dn^2}[\ell n\ c] \qquad (11)$$

where d^2/dn^2 is defined in the "straight line" sense via the progression between the last two lines of Equation 11. Carrying out the differentiation of (ℓn c) gives the alternative form

$$\frac{d}{ds}\left(\frac{1}{R_w}\right) = \frac{1}{cR_w}\ \frac{dc}{ds} - \frac{1}{c}\frac{d^2c}{dn^2} - \frac{1}{R_w^2} \qquad (12)$$

where

$$\frac{d^2c}{dn^2} = c_{xx} \sin^2\theta - 2c_{xy} \sin\theta \cos\theta + c_{yy} \cos^2\theta \qquad (13)$$

Suppose now that the source is located at some point on the (negative) y axis. At each point along a ray we know the range x, the slope angle θ, and the wave front curvature $1/R_W$ (as a result of Equation (12)). Let F denote the intensity (energy rate per unit area) along a ray. It now follows from simple geometry that

$$-\frac{1}{F}\frac{dF}{ds} = \frac{\cos\theta}{x} + \frac{1}{R_w} \qquad (14)$$

If A(x, y) denotes the acoustic attenuation in the water, then the final equation becomes

$$-\frac{1}{F}\frac{dF}{ds} = \frac{\cos\theta}{x} + \frac{1}{R_w} + A(x,y) \qquad (15)$$

In a program, it is worthwhile to record each term in Equation (15) separately; thus, F is divided into the three terms F_R, F_W, and F_A

via

$$F = F_R \cdot F_W \cdot F_A$$

so that

$$\frac{1}{F_R}\frac{dF_R}{ds} = \frac{\cos\theta}{x} = \frac{1}{x}\frac{dx}{ds}$$

$$\frac{1}{F_W}\frac{dF_W}{ds} = \frac{1}{R_W} \qquad (16)$$

$$\frac{1}{F_A}\frac{dF_A}{ds} = A(x, y)$$

The first of these equations yields

$$F_R = \frac{\text{const.}}{x}$$

when the constant is chosen to be the intensity of the source at unit distance (i.e., s = 1), along the chosen ray; thus, F_W and F_A are each unity at that point.

A knowledge of F_W has an interesting physical interpretation. Consider two rays emanating from the source at angle θ_0, at an incremental angle $d\theta_0$ apart. At unit distance from the source, $F_W = 1$. At a terminal point x_t, where the slope angle is θ_t and the value of F_W is F_{Wt}, we can use the fact that F_W is inversely proportional to the normal spacing dn between adjacent rays to write

$$(1)(1)d\theta_0 = F_{Wt}|dn| \qquad (17)$$

so that $|dn/d\theta_0| = 1/F_{Wt}$

2.2 CORRECTIONS TO RAY ACOUSTICS

Let (x_1, y_1, z_1) be rectangular Cartesian coordinates and t be time. Let ℓ be some characteristic length (e.g., water depth), and define the non-dimensional coordinates by $x = x_1/\ell$, etc. Consider the wave equation

$$\Delta\phi = \frac{\ell^2}{c^2}\,\phi_{tt} \tag{18}$$

where ϕ is the velocity potential, $c = c(x, y, z)$, a function of the space coordinates. Let c_o be some constant which can be taken approximately as the average value of c over the region of interest.

For periodic motion we assume

$$\phi = \mathrm{Re}\,\{u\, e^{i\omega t}\} \tag{19}$$

where ω is the (constant) angular frequency; $u(x, y, z)$ is the complex amplitude. Substitution of Equation (19) into (18) shows that u satisfies the equation

$$\Delta u + k^2 n^2 u = 0 \tag{20}$$

where

$$\Delta = \frac{\partial^2}{\partial x^2} + \frac{\partial^2}{\partial y^2} + \frac{\partial^2}{\partial z^2}, \qquad k = \frac{\ell\omega}{c_o} \qquad \text{and} \qquad n = \frac{c_o}{c}$$

The quantity k is non-dimensional and in practice k^2 is usually >>1. For example, at a frequency of 20 Hz and with a depth of 2,000 feet, k^2 is approximately 2500.

In acoustic propagation problems one is often dealing with a sequence of progressing waves of approximately constant phase; for example, plane waves, $u = e^{ikx}$, and spherical waves, $u = e^{-ikr}/r$. For such problems a natural substitution is

$$u = \alpha(x, y, z)e^{ik\beta(x,y,z)} \tag{21}$$

where the function $\beta(x, y, z)$ is to provide the travelling wave character. Substitution of Equation (21) into (20) gives

$$k^2[n^2-(\beta_x^2+\beta_y^2+\beta_z^2)]\alpha + ik[2(\alpha_x\beta_x+\alpha_y\beta_y+\alpha_z\beta_z) + \alpha\Delta\beta] + \Delta\alpha = 0 \qquad (22)$$

For large k the first term is dominant so that as a first approximation

$$\beta_x^2 + \beta_y^2 + \beta_z^2 = n^2 \qquad (23)$$

This is the eikonal equation, and its characteristics are the acoustic rays. If s is the distance along a characteristic, the differential equations of a characteristic become

$$\frac{dx}{ds} = \frac{\beta_x}{n}\ , \quad \frac{dy}{ds} = \frac{\beta_y}{n}\ , \quad \frac{dz}{ds} = \frac{\beta_z}{n}$$

$$\frac{d\beta_x}{ds} = n_x, \quad \frac{d\beta_y}{ds} = n_y, \quad \frac{d\beta_z}{ds} = n_z$$

$$\frac{d\beta}{ds} = n \qquad (24)$$

from which the conventional ray equation follows:

$$\frac{d^2x}{ds^2} = \frac{1}{n}\frac{dx}{ds}\left(n_x\frac{dx}{ds} + n_y\frac{dy}{ds} + n_z\frac{dz}{ds}\right) + \frac{1}{n}n_x \qquad (25)$$

The term that is next important in (22) can also be put to zero to get a second approximation by choosing α such that

$$2(\alpha_x\beta_x + \alpha_y\beta_y + \alpha_z\beta_z) + \alpha\Delta\beta = 0 \qquad (26)$$

From (24) and (26) it follows along a ray

$$2n\frac{d\alpha}{ds} + \alpha\Delta\beta = 0 \qquad (27)$$

i.e., $$\text{div}\ (\alpha^2\ \text{grad}\ \beta) = 0 \qquad (28)$$

and by the divergence theorem for a closed surface S

$$\int_S \alpha^2 \, \text{grad}\, \beta \cdot dS = 0 \tag{29}$$

Consider a section of a ray tube and make use of (29). The contribution to the integral from the tube sides is zero since grad β is in the direction of the ray; so that if the two end sections of the ray tube be given the indices 1 and 2, we have

$$\int_{S_1} \alpha^2 n dS = \int_{S_2} \alpha^2 n dS \tag{30}$$

Since the rate of the energy propagation per unit area is proportional to (amplitude) /c, (30) implies that the rate of energy propagation is constant along a ray tube.

This leads to the conclusion that the use of ray theory is equivalent to the omission of the last term in (22). One way of examining the adequacy of the ray theory is to solve the problem by ray theory to obtain α and β at each point and to examine the magnitude of $\Delta\alpha$. Another approach is to iterate, compute $\Delta\alpha = f$, say, and recompute α by

$$2n\frac{d\alpha}{dS} + \alpha\Delta\beta + \frac{1}{ik} f = 0 \tag{31}$$

A comparison of the revised values of α should provide a criterion for the adequacy of the ray approximation.

Such iterations can be carried out more systematically by using the asymptotic expansion below.

$$\alpha = \alpha^{(0)} + \frac{1}{ik}\alpha^{(1)} + \left(\frac{1}{ik}\right)\alpha^{(2)} + \ldots, \tag{32}$$

Substitution into (22) with β still satisfying (23) yields the sequence of equations:

$$2n\frac{d\alpha^{(0)}}{ds} + \alpha^{(0)}\Delta\beta = 0$$

$$2n\frac{d\alpha^{(1)}}{ds} + \alpha^{(1)}\Delta\beta + \Delta\alpha^{(0)} = 0$$

$$2n\frac{d\alpha^{(2)}}{ds} + \alpha^{(2)}\Delta\beta + \Delta\alpha^{(1)} = 0 \qquad (33)$$

so that $\alpha^{(0)}$, $\alpha^{(1)}$, . . ., may be determined in succession. Note that the ray paths are unaffected by this iterative procedure.

2.3 NORMAL MODES

We summarize here some of the relations between the methods of ray tracing, normal modes, and image methods.

Consider first the problem of an infinite ocean of constant depth, in which $c = c(z)$. Let there be a concentrated source, of angular frequency ω, at a distance d below the surface, and introduce a coordinate system as shown:

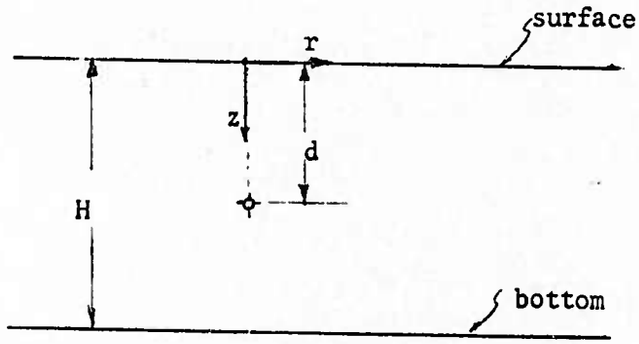

Fig. 3

Writing $\phi = \psi(r,z)e^{i\omega t}$, the governing equation becomes

$$\psi_{rr} + \frac{1}{r}\psi_r + \psi_{zz} + \frac{\omega^2}{c^2}\psi = \frac{\delta(r-\varepsilon)\,\delta(z-d)}{2\pi\varepsilon} \tag{34}$$

where $\varepsilon > 0, \varepsilon \to 0$. Here $\delta(x)$ is the delta function. As boundary conditions we will take the special situation:

$$\psi(r, 0) = 0,$$

$$\psi_z(r, H) = 0, \tag{35}$$

in order to simplify comparisons between the various methods.

(1) Normal Mode Method

We write $\psi(r, z) = \sum a_n(r)\, f_n(z)$ where $f_n(z)$ are appropriate expansion functions chosen by the use of the associate Sturm-Liouville problem:

$$\begin{cases} f'' + \left(\dfrac{\omega^2}{c^2} - \dfrac{\omega^2}{c_0^2} + \lambda\right) f = 0 \\ f(0) = 0, \\ f'(H) = 0. \end{cases} \tag{36}$$

Here c_0 is a constant equal to some average value of $c(z)$. Denote the eigenvalues by λ_n, $n = 1, 2, \ldots$, and the corresponding eigenfunctions by $f_n(z)$. Note that if $c(z) = c_0$, we have $\lambda_n = (2n-1)^2\pi^2/(2H)^2$ and $f_n = \sin(\lambda_n^{\frac{1}{2}} z)$. The orthogonality condition requires

$$\int_0^H f_m\, f_n\, dz = 0 \qquad \text{for } \lambda_m \neq \lambda_n \tag{37}$$

Let

$$\int_0^H f_n^2\, dz = g_n, \tag{38}$$

then

$$a_n(r) = \frac{1}{g_n} \int_0^H \psi(r, z) f_n(z) dz \tag{39}$$

Multiplying Equation (34) by $f_n(z)/g_n$ and integrating, we obtain by integration by parts

$$a''_n + \frac{1}{r} a'_n + \left(\frac{\omega^2}{c^2_0} - \lambda_n\right) a_n = \frac{\delta(r-\varepsilon)}{2\pi\varepsilon} \frac{f_n(d)}{g_n} \tag{40}$$

If $\lambda_n < \omega^2/c^2_0$ (say for $n < N$), the solution is a multiple of

$$J_0\left(r \sqrt{\omega^2/c^2_0 - \lambda_n}\right) \qquad \text{for } r < \varepsilon$$

and of $H_0^{(2)}(r\sqrt{\omega^2/c^2_0 - \lambda_n})$ * for $r > \epsilon$;

matching the condition at $r = \epsilon$, and permitting $\epsilon \to 0$ leads to

$$a_n(r) = -\frac{f_n(d)}{4ig_n} H_0^{(2)}(r\sqrt{\omega^2/c^2_0 - \lambda_n}) \quad \text{for } n < N \qquad (41)$$

Here N is the upper limit of values of n for which $\omega^2/c^2_0 > \lambda_n$. Similarly, for $n > N$, we obtain

$$a_n(r) = -\frac{f_n(d)}{2\pi g_n} K_0(r\sqrt{\lambda_n - \omega^2/c^2_0} \qquad n > N \qquad (42)$$

For large r, K_0 is exponentially small so that these modes are relatively unimportant.

As a numerical example, consider again $c = c_0 = 5000$ ft/sec., say, and take $\omega/c_0 = 2\pi(10)/5000 = 2\pi/500$. Then $\lambda_n = [(2n-1)\pi/(2H)]^2$. Let $H = 1000$ feet; then $f_n = \sin\sqrt{\lambda_n}\, z$, $g_n = H/2$, and

$$\psi(r,z) = \sum_1^4 \left(-\frac{1}{2iH} \sin\sqrt{\lambda_n}\, d\right) H_0^{(2)}(r\sqrt{\omega^2/c^2_0 - \lambda_n}) \sin\sqrt{\lambda_n}\, z$$

$$+ \sum_5^\infty \left(-\frac{1}{\pi H} \sin\sqrt{\lambda_n}\, d\right) K_0(r\sqrt{\lambda_n - \omega^2/c^2_0}) \sin\sqrt{\lambda_n}\, z \qquad (43)$$

The ratio of mode 5 to 4 is of the order

$$K_0\left(\frac{\pi}{2000}\sqrt{17}r\right) \Big/ H_0^{(2)}\left(\frac{\pi}{2000}\sqrt{15}\, r\right) \approx e^{-\frac{r}{200}} \qquad (44)$$

for large r, so that for r beyond 1000 feet, say, we can neglect all modes beyond the fourth. For a frequency of 1 cps in this example, all modes decay exponentially; for a frequency of 1000 cps, 400 modes are required.

* We choose $H_0^{(2)}$ rather than $H_0^{(1)}$ in order to obtain asymptotically an outgoing wave for large r, in conjunction with the time factor $e^{i\omega t}$.

(2) Images or Rays

A delta function source at (x_0, y_0, z_0) in an infinite medium satisfies the equation (for $c(z) = c_0$):

$$\Delta\psi + \frac{\omega^2}{c_0^2}\psi = \delta(x - x_0)\ \delta(y - y_0)\ \delta(z - z_0) \tag{45}$$

Let ρ denote the distance from this source; then

$$\psi = -\frac{1}{4\pi\rho}\, e^{-\frac{i\omega\rho}{c_0}} \tag{46}$$

(Even for $c = c(z)$ this is adequate for small ρ).

The problem considered on Page 11 can be interpreted in terms of coupled pairs of images; for the case $c(z) = c_0$, the analysis is particularly easy:

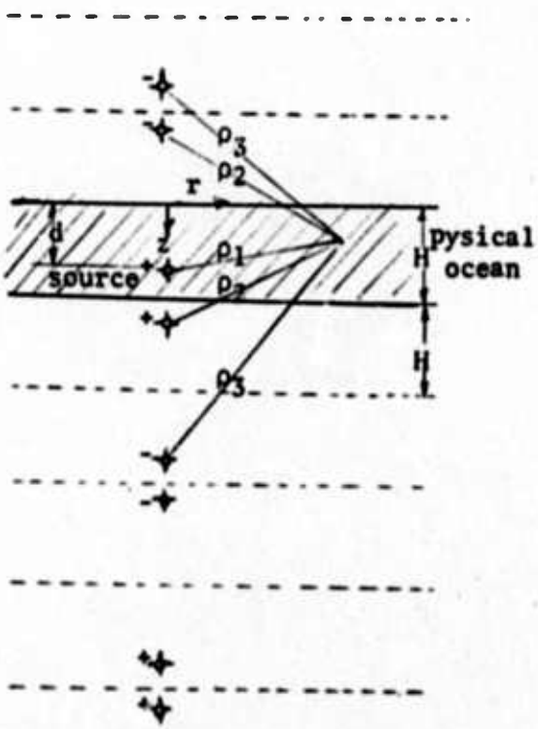

Fig. 4

It follows that

$$\psi = -\frac{1}{4\pi}\left\{\frac{1}{\rho_1} e^{-\frac{i\omega\rho_1}{c_0}} + \frac{1}{\rho_2} e^{-\frac{i\omega\rho_2}{c_0}} - \frac{1}{\rho_3} e^{-\frac{i\omega\rho_3}{c_0}} - \frac{1}{s_2} e^{-\frac{i\omega s_2}{c_0}} \cdots \right. \tag{47}$$

This solution is identical with that obtained by the ray method since there is perfect reflection at top and bottom with a phase change of π at the top surface. Besides, the following relations hold:

$$\begin{cases} \rho_1^2 = r^2 + (z - d)^2 \\ \rho_2^2 = r^2 + (H - z + H - d)^2 \\ \text{----------} \\ s_2^2 = r^2 + (z + d)^2 \end{cases} \tag{48}$$

Advantage can be taken of the phase differentials to simplify the summation of Equation (47)

(3) Hankel Transform

In some layer problems, preliminary Fourier decomposition in z-direction may be awkward. An alternative method is that of Henkel transform which will be made use of to illustrate this problem. Returning to Equation (34) define

$$\psi(\rho,z) = \int_0^\infty r\, J_0(r\rho)\psi\ (r,z)dr \tag{49}$$

and (34) then implies

$$\psi_{zz} + (\frac{\omega^2}{c^2} - \rho^2)\psi = \frac{1}{2\pi}\,\delta(z-d) \tag{50}$$

which is an ordinary differential equation in z.

For the case $c(z) = c_0$, we obtain

$$\psi(\rho,z) = -\frac{1}{4\pi\gamma\ \cos\gamma H}\{\sin\gamma(z+d-H) + \sin\gamma(H - |z-d|)\} \tag{51}$$

where $\gamma = \sqrt{\omega^2/c_0^2-\rho^2}$.

In any event, whether $c = c(z)$ or $c = c_0$, we must eventually compute

$$\psi(r,\ z) = \int_0^\infty \rho\ J_0(r\rho)\ \psi(\rho,\ z)d\rho \tag{52}$$

where ψ, in (51) may well have singularities on the path of integration (where $\cos\gamma H = 0$).

There are two useful devices associated with (52). The first of these involves the addition of a small amount of damping to the wave equation predecessor of (34), so as to eventually move the singularities off the path of integration. This results in the term (ω^2/c^2) in (34) becoming replaced by $(\omega^2/c^2 - \epsilon i)\psi$, where ϵ is a small positive parameter; eventually $\epsilon \to 0$. The effect of this in the special case (51) is to locate the singularities at

$$\rho = \pm \sqrt{\omega^2/c^2 - \varepsilon i - ((2n-1)\pi/2H)^2} \tag{53}$$

for integral values of n. These are a finite number lying just below the positive real axis, an infinite number lying just to the right of the negative imaginary axis and also at the negatives of all these positions.

The second device is to recognize that, in (52), we can write

$$J_0(r\rho) = \frac{1}{2}\{H_0^{(1)}(r\rho) + H_0^{(2)}(r\rho)\}, \tag{54}$$

where we will choose the branch cut of the Hankel functions to lie in the upper half ρ-plane. Then as we move continuously from the positive to the negative real axis through the negative half plane, we find that for $\alpha > 0$,

$$H_0^{(2)}(-r\alpha) = -H_0^{(1)}(r\alpha),$$

so that (52) becomes

$$\psi(r,z) = \frac{1}{2}\int_0^\infty \rho\, H_0^{(1)}(r\rho)\, \psi(\rho,z)d\rho + \frac{1}{2}\int_0^\infty \rho\, H_0^{(2)}(r\rho)\, \psi(\rho,z)d\rho$$

$$= -\frac{1}{2}\int_0^\infty \rho H_0^{(2)}(-r\rho)\, \psi(\rho,z)d\rho + \frac{1}{2}\int_0^\infty \rho H_0^{(2)}(r\rho)\, \psi(\rho,z)d\rho$$

$$= \frac{1}{2}\int_{-\infty}^\infty \rho H_0^{(2)}(r\rho)\, \psi(\rho,z)d\rho \tag{55}$$

where $H_0^{(2)}$ has no branch cut in the lower half plane. For the special case of (51) a straightforward residue calculation (using the device of (53) and noting that the point $\rho = \omega^2/c^2$ is not a branch point as $\varepsilon \to 0$) reproduces the results of method (1).

(4) Perturbations

An efficient way in which to handle the variable c case via normal modes would appear to be by use of perturbations. Consider the j^{th} mode in (36) and write

$$f_j'' + [\frac{\epsilon\omega^2 h(z)}{c_0^2} + \lambda_j] f_j = 0, \tag{56}$$

where $c(z) = c_0/\sqrt{1+\epsilon h(z)}$. With $0 < \epsilon << 1$ we also write

$$\begin{cases} f_j = f_j^{(0)} + \epsilon f_j^{(1)} + \epsilon^2 f_j^{(2)} + \ldots, \\ \lambda_j = \lambda_j^{(0)} + \epsilon\lambda_j^{(1)} + \epsilon^2\lambda_j^{(2)} + \ldots., \end{cases} \tag{57}$$

so as to obtain the sequence of equations

$$\begin{cases} f_j^{(0)''} + \lambda_j^{(0)} f_j^{(0)} = 0 \\ f_j^{(1)''} + \lambda_j^{(0)} f_j^{(1)} = -hf_j^{(0)} - \lambda_j^{(1)} f_j^{(0)} \\ f_j^{(2)''} + \lambda_j^{(0)} f_j^{(2)} = -hf_j^{(1)} - \lambda_j^{(1)} f_j^{(1)} - \lambda_j^{(2)} f_j^{(0)} \end{cases} \tag{58}$$

The boundary conditions are

$$f_j^{(p)}(0) = f_j^{(p)'}(H) = 0 \quad \text{for all } p. \tag{59}$$

It follows that $\lambda_j^{(0)} = (2j-1)^2\pi^2/4H^2$ and that $f_j^{(0)} = \sin((2j-1)\pi z/2H)$. Because of the structure of the second of (58), there can be a solution only if its right-handed side is orthogonal to $f_j^{(0)}$, thus $\lambda_j^{(1)}$ must be given by

$$\lambda_j^{(1)} = -\frac{2}{H}\int_0^H h(z)\sin^2\frac{(2j-1)\,z}{2H}\,dz \tag{60}$$

We can now find $f_j^{(1)}$, discarding any multiple of $f_j^{(0)}$ which might appear. For example, let $h(z) = z$, $\mu = (2j-1)\pi/2H$, then

$$\lambda_j^{(1)} = -\frac{H}{2}\left[1 + \frac{1}{H^2\mu^2}\right], \tag{61}$$

and

$$f_j^{(1)} = \frac{z^2+2\lambda_j^{(1)}z}{4\mu}\cos\mu z - \frac{z}{4\mu^2}\sin\mu z \tag{62}$$

In Equation (41) we now obtain a value for $a_n(r)$, correct to order ε, by replacing λ_n by $\lambda_n^{(0)} + \varepsilon\lambda_n^{(1)}$, $f_n(d)$ by $f_n^{(0)}(d) + \varepsilon f_n^{(1)}(d)$ and by revising g_n appropriately. Higher order corrections may be obtained similarly: of course, in this special case an exact analytical solution is also available but our main purpose was to outline the general perturbation technique.

2.4 FOCAL ZONES AND CAUSTICS

In the neighborhood of a focal zone or caustic some distance from a source in a cylindrically symmetric problem the motion may be considered two-dimensional.

Consider first a focusing situation in which a ray bundle is approaching the origin. We write $\phi = \mathrm{Re}\,(ue^{i\omega t})$ with

$$\Delta u + k^2 u = 0 \tag{63}$$

where $k = \omega/c$; we take c as constant in the neighborhood of the focus. A plane wave solution of (63) is given in polar coordinates by

$$u(r, \theta) = e^{ikr\cos(\theta-\gamma)} \tag{64}$$

where γ is the angular direction from which the wave is coming. A superposition of such waves is also a solution; consider therefore a wave bundle of the form:

$$u(r, \theta) = \int_0^{\Gamma} f(\gamma) e^{ik[m(\gamma)+r\cos(\theta-\gamma)]}\, d\gamma \tag{65}$$

where $f(\gamma)$ and $m(\gamma)$ are arbitrary real functions. Here Γ is to be the angle within which rays approach the origin.

A useful tool in dealing with integrals like that in (65) is the method of stationary phase which states that if there is one point, t_0, in the interval (a, b) at which $h'(t) = 0$, then for large $\lambda > 0$,

$$\int_a^b e^{i\lambda h(t)}\, g(t)\, dt \simeq \sqrt{\frac{2\pi}{\lambda|h''(t_0)|}}\, g(t_0) e^{i\lambda h(t_0) \pm i\pi/4} \tag{66}$$

where the $\pm$ sign is chosen for $h''(t_0) > 0$ or < 0, respectively (Reference 1).

For large values of r, Equation (64) thus implies

$$u(r, \theta) \sim \sqrt{\frac{2\pi}{kr}}\ f(\theta) e^{ik[m(\theta)+r]-i\pi/4} \tag{67}$$

for $0 < \theta < \Gamma$; for θ outside this range (and outside the range $0 < \theta-\pi < \Gamma$), we have $u(r, \theta) \sim 0$ (relatively). Thus, the exact solution (65) corresponds to a ray bundle of aperture Γ. Let us choose the bundle aperture sufficiently small that $f(\theta)$ (the amplitude factor) is constant; we will also make the slight additional simplification $m(\theta) = \text{constant}$. Then

$$u(r, \theta) = f\, e^{ikm} \int_0^{\Gamma} e^{ikr \cos(\theta-\gamma)}\, d\gamma \tag{68}$$

where f and k are found from the amplitude and phase of u at some large distance r, as given by (67).

We observe first that on the other side of the focal point, the method of stationary phase can also be applied to give, for large r,

$$u(r, \theta) \sim \sqrt{\frac{2\pi}{kr}}\ f\, e^{ik(m-4)+i\pi/4} \tag{69}$$

The change in sign of the r term in the exponent simply corresponds to the fact that the waves are now outgoing rather than incoming; the change from $-\pi/4$ to $\pi/4$ means that the phase has advanced by $\pi/2$ in the passage through the focus. Observe, however, that apart from these effects there is no amplitude change; the energy flow rate between a pair of converging rays is the same as that between the corresponding pair of diverging rays.

Equation (67) is, of course, not valid at the focal point itself--it would give $u = \infty$. However, (68) is valid everywhere so that at $r = 0$

$$u = f\, e^{ikm}\, \Gamma \tag{70}$$

Thus the ratio $u(0)/u(r)$, r large, is given by

$$\frac{u(0)}{\sqrt{r}\,u(r)} \approx \sqrt{\frac{k}{2\pi}}\ (e^{-ikr+i\pi/4})\Gamma \tag{70}$$

for a ray bundle of aperture Γ, (the factor $\sqrt{r}$ simply reflects the fact that $u(r) \approx 1/\sqrt{r}$ as we move along a ray). Values of u at other points in the immediate neighborhood of the focus can be found by numerical or approximate evaluation of (68). Note that u_r, u_{rr}, etc., are easy to find at $r = 0$.

Consider next the case of a caustic. A caustic will have curvature, so let the caustic be a circular arc (Fig. 6), with radius R.

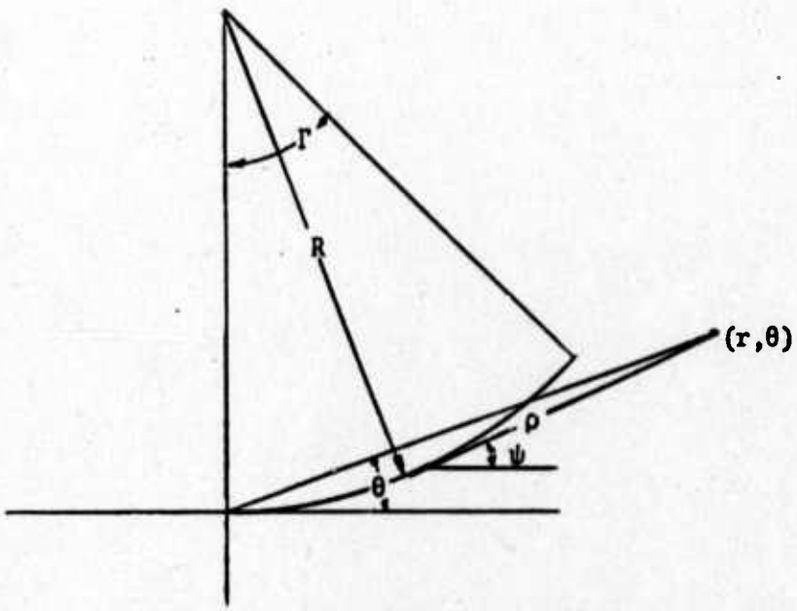

Fig. 6

Any point in the plane may be designated in terms of polar coordinates (r,θ); we will also use the tangent-arc coordinates (ρ,ψ) as shown. Thus,

$$\begin{cases} r\cos\theta = R\sin\psi + \rho\cos\psi \\ r\sin\theta = R(1-\cos\psi) + \rho\sin\psi \end{cases} \tag{72}$$

Some useful identities are

$$\begin{cases} r^2 = 2R^2 - 2R^2\cos\psi + \rho^2 + 2R\rho\sin\psi \\ r\sin(\psi-\theta) = R(1-\cos\psi) \\ r\cos(\psi-\theta) = R\sin\psi + \rho \\ r = R\sin\theta + R\sin(\psi-\theta) + \rho\cos(\psi-\theta) \\ \rho\sin(\psi-\theta) + R\cos\theta - R\cos(\psi-\theta) = 0 \end{cases} \tag{73}$$

We also have

$$\begin{cases} \psi_r = -\sin(\psi-\theta)/\rho \\ \psi_\theta = r\cos(\psi-\theta)/\rho \\ \rho_r = (r-R\sin\theta)/\rho \\ \rho_\theta = -r\,R\cos\theta/\rho \end{cases} \tag{74}$$

Moreover, for any function $\nu(\rho,\psi)$

$$\Delta\nu = (1+\frac{R^2}{\rho^2})\nu_{\rho\rho} - \frac{2R}{\rho^2}\nu_{\rho\psi} + \frac{1}{\rho^2}\nu_{\psi\psi} + (\frac{1}{\rho} - \frac{R^2}{\rho^3})\nu_\rho + \frac{R}{\rho^3}\nu_\psi \tag{75}$$

Again, we try to find an exact solution of (63) which, in the ray approximation, has the above circular arc as a caustic. We try

$$u(r, \theta) = \int_0^{\Gamma} f(\gamma)\, e^{i[m(\gamma)+r\cos(\theta-\gamma)]}\, d\gamma \tag{76}$$

as before. Using (67) we see that at large values of r ($0 < \theta < \Gamma$), a curve of constant phase satisfies $r + m(\theta) = \text{constant}$. A vector tangential to this curve has (x, y) components parallel to $(-m'(\theta)\cos\theta - r\sin\theta,$ $-m'(\theta)\sin\theta + r\cos\theta)$. Since a vector in the ray direction has components $(\cos\psi\ ,\ \sin\psi)$, the orthogonality condition becomes

$$\cos\psi[-m'(\theta)\cos\theta - r\sin\theta] + \sin\psi\,[-m'(\theta)\sin\theta + r\cos\theta] = 0 \tag{77}$$

or

$$-m'(\theta)\cos(\theta-\psi) + R(1-\cos\psi) = 0 \tag{78}$$

But at large r, $\theta \approx \psi$, so we must require

$$m'(\theta) = R(1-\cos\psi) \tag{79}$$

whence

$$m(\theta) = R\theta - R\sin\theta \tag{80}$$

(the constant of integration is absorbed into $f(\theta)$). We next set

$$f(\theta) = \sqrt{\frac{kA}{2\pi}}\ e^{i\pi/4} \tag{81}$$

in order to obtain an amplitude at a large reference distance A of

$$u(A, \theta) \sim e^{ik[R(\theta-\cos\theta)+A]} \tag{82}$$

for $0 < \theta < \Gamma$. Then

$$u(r,\theta) = \sqrt{\frac{kA}{2\pi}}\; e^{i\pi/4} \int_0^{\Gamma} e^{ik[R(\gamma-\sin\gamma) + r\cos(\theta-\gamma)]}\, d\gamma \tag{83}$$

or in terms of ρ and ψ,

$$u(\rho,\psi) = \sqrt{\frac{kA}{2\pi}}\; e^{i\pi/4} \int_0^{\Gamma} e^{ik[R\gamma+R\sin(\psi-\gamma)+\cos(\psi-\gamma)]}\, d\gamma \tag{84}$$

This is now an exact solution of the reduced wave equation; at large r the ray approximation yields rays having the desired caustic.

We are interested in $u(\rho,\psi)$ for small ρ, i.e., close to a caustic. We have to break up the calculation into two regions. In the first of these, $\rho = 0(R)$; in fact, we set $\rho = \tau R$, and let k become large holding τ fixed. For τ not too large and for ψ not too close to 0 or Γ, there are two stationary phase points in (84) and therefore

$$u \sim \sqrt{\frac{A}{R\tau}}\; e^{ikR(\psi+\tau)}\; [1 + ie^{ikR(\gamma_0-\psi-2\tau)}] \tag{85}$$

where γ_0 is defined by

$$\tan[\gamma_0-\psi)/2] = \tau \tag{86}$$

The inverse of $\sqrt{\tau}$ implies that this solution breaks down near $\tau = 0$. To handle the small τ region, we use a boundary layer method. Set

$$u = \alpha(x, y)\; e^{ik(R\psi+\rho)} \tag{87}$$

in (63) to obtain

$$ik(2\alpha_\rho + \frac{1}{\rho}\alpha) + (1 + \frac{R^2}{\rho^2})\alpha_{\rho\rho} - \frac{2R}{\rho^2}\alpha_{\rho\psi}$$
$$+ \frac{1}{\rho^2}\alpha_{\psi\psi} + (\frac{1}{\rho} - \frac{R^2}{\rho^3})\alpha_\rho + \frac{R}{\rho^3}\alpha_\psi = 0 \tag{88}$$

If we discarded all terms except the first (for large k), then α would clearly be singular at $\rho = 0$. We therefore set $\rho = k^{-s}\xi$, with $s > 0$; a substitution into (88) indicates that we must choose $s = 1/3$. The lowest order part of the boundary layer equation thus becomes

$$i(2\alpha_\xi + \frac{1}{\xi}\alpha) + \frac{R^2}{\xi^2}\alpha_{\xi\xi} - \frac{R^2}{\xi^3}\alpha_\xi = 0 \tag{89}$$

whose solution has been given in terms of Airy functions by Buchal and Keller (Reference 2) as

$$u = c_1 \alpha^{(1)} + c_2 \alpha^{(2)} \tag{90}$$

$$\begin{cases} \alpha^{(1)} = \exp(-\frac{i\xi^3}{3R^2})\ \mathrm{Ai}(2^{-2/3} R^{-4/3} \xi^2 e^{-i\pi/3}) \\ \alpha^{(2)} = \exp(-\frac{i\xi^3}{3R^2})\ \mathrm{Ai}(2^{-2/3} R^{-4/3} \xi^2 e^{i\pi/3}) \end{cases} \tag{91}$$

The behavior of α for large ξ must be the same as its behavior from (85) for small τ, if there is to be an overlap region. After some algebra, this requirement yields:

$$\begin{cases} c_1 = e^{-i\pi/12}\ 2^{5/6}\ \sqrt{\pi A}\ R^{-1/3}\ k^{1/6} \\ c_2 = i\ e^{i\tau/12}\ 2^{5/6}\ \sqrt{\pi A}\ R^{-1/3}\ k^{1/6} \end{cases} \tag{92}$$

In particular, the value of u on the caustic itself will be

$$6^{-1/6}\ A^{1/2}\ \pi^{-1/2}\ R^{-1/3}\ k^{1/6}\ \Gamma(\tfrac{1}{3})\ e^{i\pi/4} \tag{93}$$

REFERENCES

1. Carrier, G., Krook, M., Pearson, C., Functions of a Complex Variable, McGraw-Hill, 1966, p.273.

2. Buchal, R. N. and Keller, J. B., "Boundary Layer Problems in Diffraction Theory," *Communications of Pure and Applied Mathematics*, Vol. 13, 1960, p.85.

3. THE ARCTIC OCEAN ENVIRONMENT FOR UNDERWATER ACOUSTIC STUDIES

The principal features of the Arctic Ocean environment of concern for studies of long range underwater sound propagation are bottom topography and composition, ice cover roughness distribution and sound speed profile distribution. The sound speed profile is in turn determined by the local temperature and salinity profiles. Additional areas of concern for acoustic propagation studies are in the problems of propagation losses which are determined by sea water absorption and scattering, surface (ice cover) reflection and absorption and bottom reflection and absorption.

In this discussion we will review the current knowledge of these topics as available from the open literature. Extensive, up to date and comprehensive information on acoustic propagation experiments in the Arctic Ocean as well as on topography is available in the classified literature. The two references of interest here, References 1 and 2, deal with topography and transmission experiments which represent the current knowledge as of December 1972, Reference 3. A case should be made here for declassification of the classified topographical charts to make more comprehensive and uniform data available to the general scientific community.

3.1 BOTTOM TOPOGRAPHY

The Arctic Basin may be divided into two primary topological areas: that comprised of continental shelves forming about two-thirds of the total area and that forming the central basin. The continental shelf north of Eurasia is the widest in the world extending up to 850 km width in the Barents Sea. This shelf is cut by deep re-entrants north of Europe--the best known are the Svataya Anna and Voronin Troughs--and a marked absence of troughs north of Asia. North of Alaska and the Chukchi Sea there are three submarine canyons, two leading into the Chukchi Plain and one, Barrow Canyon, leading into the Canada Basin. The shelf north of Canada is characterized by deep passages among the islands of the archipelago leading from the rather rugged structural highs rising from the floor of the central basin.

The central Arctic is divided by three submarine mountain ranges into four basins. These mountain ranges run roughly parallel to each other and are aligned to 150° - 330° * longitude. The central range is the Lomonosov Ridge very nearly crossing the pole; this feature is very narrow, only about 40 km wide at the narrowest point, with crest depths of 850 to 1200 meters. On the Alaskan side of the Ridge lies the Markarov Basin (Wrangel and Fletcher abyssal plains) and on the European side, the Fram Basin (Pole Abyssal Plain). In turn, the Fram Basin is separated from the Nautilus Basin (Barents abyssal plain) by the Nansen Cordillera (Mid-Oceanic Ridge). The previously noted Svataya Anna and Voronin Troughs lead into the Nautilus Basin between the surface features Severnaya Zemlya and Franz Josef Land. Toward the Alaska-Canada side of the Lomonosov Ridge there is the dominant Alpha Cordillera (known as the Mendeleev Ridge in USSR) which separates the Markarov Basin from the extensive Canada Basin (Beauford Deep). The Alpha Cordillera is a rather broad mountainous feature which expands to join the Lomonosov Ridge north of Greenland; the rugged terrain emanating from the Canadian Arctic Archipelago can be thought of as focusing toward the Alpha Cordillera as one moves toward the USSR.

The greatest density of bathymetric data is available for the sector 170° to 280° longitude bounded by the US-Canada-Greenland shoreline. Data have been gathered from drifting ice island stations and air lifted temporary stations as well as from ship and submarine operations. In a recent paper, Wold and Ostenso, Reference 4, present a detailed bathymetric chart of this segment with 200 meter contour intervals except 10-meter contour intervals over Chukchi shelf. The accuracy of the bathymetry data resulting from the reported survey (from 1960 through 1969) is quoted as ± 2% with location errors of ± 3 km for the ice island measurements and ± 15 km for the air lifted station measurements. Wold and Ostenso have also included "all other soundings" (Reference 4, page 6254) in compiling the contour map.

---

* Throughout this report we write 150°E longitude as 150° and 30°W as 330°

Fairly detailed bathymetry is also available for the Canadian Arctic from the Canadian charts, Reference 5. Since the sector covered includes the sector of Wold and Ostenso, these charts should be compared for consistency. A comprehensive physiographic diagram of the floor of the Arctic Ocean was prepared by Dr. Alan Beal for the U. S. Navy Electronics Laboratory in 1966 which utilized all available drift station soundings in addition to submarine soundings through 1962. Versions of this data are available in Reference 6 and 7. However, these soundings are concentrated along the tracks of the drift stations and submarines, hence, leaving large gaps in the coverage where the information must be extrapolated. An updating of this information including subsequent submarine soundings has been in progress by Beal but, for various reasons, is now at a standstill, Reference 8.

The U. S. Naval Oceanographic Office (NAVOCEANO) has bathymetric charts covering most of the world's oceans. Since NAVOCEANO is the official repository of all sounding data obtained by ships under U. S. Navy control as well as collecting data from other Government agencies and private sources, the NAVOCEANO charts are also a good source. Specific bottom profile accuracy can be improved by using information from the collection sheets (original sounding echogram entries) compiled by the Bathymetry Division, Hydrographic Surveys Department, NAVOCEANO, which are used in constructing the topographical contour maps.

3.2 SOUND-SPEED PROFILE DATA

Speed of sound in water is a function of temperature, salinity, and pressure. In the main Arctic basin the variation of temperature and salinity is such that for the most part the speed of sound profile is an increasing function of depth from the surface to the bottom. Furthermore, as noted by various investigators, References 9 and 10, the acoustic signal propagation characteristics which are governed by the sound-speed profile are quite stable both in time and geographic location indicating that the temperature and salinity profiles in the primary Arctic basin do not vary substantially.

Variations of the temperature and salinity profiles can, however, be expected near the Bering Strait and junctions with the Greenland and Norwegian Seas where the influence of Pacific and Atlantic Ocean waters is most significant (References 11, 12, and 13). As a result of the characteristic sound-speed profiles, there exists a natural half-channel wave guide in the Arctic with the axis at the underice surface or surface of open water. This Arctic wave-guide is the low frequency analog of the deep sound channel or SOFAR channel of the non-polar oceans (low frequency because the underice roughness causes loss of high frequency signals after some distance of propagation).

The prime source of sound-speed profile data in the oceans is the National Oceanographic Data Center (NODC), Reference 14. The data is stored on magnetic tape and consists of temperature, salinity and sound speed versus depth. Sound speed is calculated by Wilson's equation, Reference 15.

The NODC data file can be used to generate the sound speed field along any desired propagation path by selecting a profile data zone (determined by a strip extending to each side of the propagation path to some distance at which profiles are to be considered satisfactory for inclusion in actual path profile determination). A search program operated by NODC will then search the magnetic tape and print out those sound speed profiles taken in the month or season of interest and located in the selected data zone. Data in the file is keyed by the Marsden Square Chart.

Data on the microstructure of the sound-speed profile, as determined by temperature, salinity and pressure variations is not readily available. Current work under the AIDJEX project by Coachman, et al., Reference 18, is yielding a more detailed understanding of possible layering in the upper regions of the Arctic Ocean water mass. However, since the AIDJEX stations cover, at best, a 200 x 200 km area of the Ocean (100 km station to station distance plus maximum drift expectation), the data may not be of immediate use in long range acoustic signal propagation studies. This data enters the NODC file with about a year's delay. From the point of view of the low frequencies of interest (~ 20 Hz), the microstructure will not have significant effects.

3.3 UNDERICE CHARACTERISTICS

Since one boundary of the sound channel is formed by the ice canopy (or, on occasions, the Arctic open water surface), the characteristics of the underice surface must be known. The sound waves propagate by refraction in the deep water and repeated reflections from the ice canopy so the primary feature of interest is the underice roughness. The dominant roughness features are in the form of pressure ridges with above and below ice buildup due to the motion and resultant deformation of the Arctic ice pack. Information on the characteristic dimensions of the above-ice features (termed "sails") and underice features ("keels") has been derived from overflight observations using visual and laser profilometer techniques and submarine sonar soundings. Such information allows a compilation of sail height and keel depth distributions and also, to some extent, the distribution of spacings between the ridges. The significant papers on this data are in References 19, 20, and 21.

Since the distribution of the pressure ridges is, to current knowledge, random, a statistical description of the underice roughness is most suited for sound propagation studies. Reference 20 derives a theoretical distribution function for pressure ridge sail heights and keel depths from the assumption of randomness and also presents a distribution function for ridge spacings based on spatial randomness assumption. These distribution functions are correlated with observations with good agreement. From the distribution functions, values for the rms ice roughness may be determined to be used directly in sound propagation models. Further detail on the underice roughness will be available for limited regions of the polar pack from underice profilometer experiments currently in progress in conjunction with the AIDJEX program by the Applied Physics Laboratory, University of Washington, Seattle (Mr. Robert Francois). This data has not yet been correlated with the data and theory of References 19 and 20.

3.4 PROPAGATION LOSS

To compute the sound intensity at any listening location, one must take into account the propagation losses due to absorption in the water and by reflections

from the boundaries (ice cover and bottom) of the sound channel. The absorption loss for the low frequencies of interest in long range propagation studies is small; however, it may be calculated by extrapolation of the Marsh and Schulkin formula of Reference 22.

Thorp, Reference 23, has advocated an alternate (simpler) formula for attenuation at low frequency; however, in a review paper (Reference 24) published in March 1972, Berman and Guthrie make the observation that

> "... we find that when such a critical analysis (of experimental evidence) is made, little or no valid evidence exists to point to the existence of a low frequency absorption above that which may be extrapolated from the Marsh and Schulkin formula."

Furthermore, in view of the uncertainties of the boundary characteristics and their contribution to propagation loss, the differences in the loss coefficients are negligible.

Exceedingly little data exists on bottom reflection losses for the calculation of which bottom density and sound speed are required. In the review paper, Berman and Guthrie, speaking about ocean propagation in general, state that

> "Scant data exists on bottom reflection loss to serve as a guide for even representative models for the low frequency, low grazing angle reflections that can be expected to dominate in long range propagation by bottom bounce. It can be assumed that a ray incident on the bottom will undergo a fractional attenuation that is a function of wavelength, grazing angle, surface roughness and the geological structure of the bottom."

Information on the geological structure of the bottom could become more available with the explorations by commercial interests for mineral resources in the Arctic spurred by the oil discoveries. However, much of this information will never be available to the scientific community unless specific coordination with commercial exploration efforts is made by interested Government agencies.

The most up to date and comprehensive results on experimental studies of propagation losses in the Arctic are those given in the classified report by Buck, et al., Reference 2. Considerable relative loss data have been gathered by Kutschale and co-workers at Lamont-Doherty Laboratories, Columbia University, New York, which are useful in comparative acoustic propagation studies.

3.5 RECOMMENDATIONS FOR ACQUISITION OF REQUIRED DATA

The review of available (unclassified) literature indicates that substantially greater effort is necessary to acquire the necessary density and quality of environmental data of importance to long range sound propagation in the Arctic. Most critical shortcomings exist in the definition of bottom topology and geological structure as well as underice characteristics. The density of bathymetric data as well as the quality, can be greatly increased at reasonable cost by use of a recently developed airlift through the ice bathymetric system. Edo Western Corporation, Reference 25, has tested a prototype transducer which can be placed on the snow or ice and operated by remote control from inside a helicopter or ski plane. The battery powered system generates a high power, low frequency signal capable of penetrating ice of up to 12 feet in thickness. Depth readings of 1400 feet were encountered in the prototype test and typical time per data point was on the order of one minute. Development of rapid salinity and temperature sampling procedures would allow thorough mapping of the medium. Detailed low frequency propagation loss studies should be carried out in conjunction with the oceanographic data gathering along specified known paths using harmonic sources. Use of underice profilometers along the selected propagation paths would define more precisely the effects of underice roughness on the signals.

REFERENCES

1. U. S. Navy Hydrographic Office, 6700 Series Arctic Topography Charts.

2. Buck, B., et al., "Underwater Acoustic Experiments at Three Manned Stations in the Central Arctic--Apring 1970", Office of Naval Research, Code 466 Undersea Branch, TR-70-101, December 1970.

3. Personal communication, Bo Buck, Delco, Santa Barbara, 805-968-2602.

4. Wold, R. J. and Ostenso, N. A., "Gravity and Bathymetry Survey of the Arctic and Its Geodetic Implications," *Journal of Geophysical Research*, Volume 76, No. 26, September 10, 1971.

5. Arctic Bathymetry Map, Canadian Hydrographic Service, 1966-1967, (72°N, 270°-360° and 72°N, 180°-270°).

6. Beal, M. A., Edvaldson, F., Hunkins, K., Molloy, A., and Ostenso, N., "The Floor of the Arctic Ocean: Geographic Names," *Arctic*, 19, 1966.

7. Beal, M. A., "Bathymetry and Structure of the Arctic Ocean," Ph.D. Thesis, Oregon State University, Corvallis, 1968.

8. Personal communication, Dr. Alan Beam, Oceanographer, Arctic Submarine Laboratory, Naval Undersea Research and Development Center, San Diego, California, 714-225-7951.

9. Kutschale, H., "Arctic Hydroacoustics," *Arctic*, Vol. 22, No. 3, September 1969.

10. Marsh, H. W. and Mellen, R. H., "Underwater Sound Propagation in the Arctic Ocean," *The Journal of the Acoustical Society of America*, Vol. 35, No. 4, April 1963.

11. Coachman, L. K. and Barnes, C. A., "The Contribution of Bering Sea Water to the Arctic Ocean," *Arctic*, Vol. 14, 1961.

12. Coachman, L. K. and Barnes, C. A., "The Movement of Atlantic Water in the Arctic Ocean," *Arctic*, Vol. 16, 1963.

13. Kinney, P., Arhelger, M. E. and Burrell, D. C., "Chemical Characteristics of Water Masses in the Amerasian Basin of the Arctic Ocean," *Journal of Geophysical Research*, Vol. 75, No. 21, July 20, 1970.

14. Odum, W. Henry, Data Services Branch, U. S. Department of Commerce NOAA, NODC, Rockville, Maryland 20852.

15. Wilson, W. D., "Equation for the Speed of Sound in Sea Water," *The Journal of the Acoustical Society of America*, Volume 32, No. 10, October 1960.

16. Leroy, C. C., "Formulas for the Calculation of Underwater Pressure in Acoustics," *The Journal of the Acoustical Society of America*, Vol. 14, No. 2, August 1968.

17. Leroy, C. C., "Development of Simple Equations for Accurate and More Realistic Calculation of the Speed of Sound in Sea Water," NATO TR No. 128, Saclant ASW Research Centre, La Spegia, Italy, November 1968.

18. AIDJEX Office, Division of Marine Resources, University of Washington, 4059 Roosevelt Way, NE, Seattle, Washington.

19. Wittmann, W. and Schule, J. J., "Comments on the Mass Budget of Arctic Pack Ice," *Proceedings Symposium on Arctic Heat Budget and Atmospheric Circulation*, Rand Corporation, (RM-5233-NSF) 215-246, 1966.

20. Weeks, W. F., Kovacs, A., and Hibler III, W.D., "Pressure Ridge Characteristics in the Arctic Coastal Environment," *Proceedings First International Conference on Port and Ocean Engineering Under Arctic Conditions* (Technical University Norway, 23-30, August 1971), p. 32, 1972.

21. Hibler III, W.D., Weeks, W. F., and Mock, S. J., "Statistical Aspects of Sea Ice Ridge Distributions," U. S. Army Cold Regions Research and Engineering Laboratory, Hanover, New Hampshire 03755.

22. Schulkin, M. and Marsh, H. W., "Sound Absorption in Sea Water," *The Journal of the Acoustical Society of America*, Vol. 34, No. 6, June 1962.

23. Thorp, W. H., "Analytical Description of the Low Frequency Attenuation Coefficient," *The Journal of the Acoustical Society of America*, Vol. 42 No. 1, July 1967.

24. Berman, A. and Guthrie, A. N., "On the Medium from the Point of View of Underwater Acoustics," *The Journal of the Acoustical Society of America*, Vol. 51, No. 3, Part 2, March 1972.

25. Edo Western Corporation, 2645 2nd West, Salt Lake City, Utah 84115, 801-486-7481.

4. APPLICATION OF RAY ACOUSTICS IN THE ARCTIC

The factors that affect underwater sound propagation are the nature of the sound speed depth profile, bottom and surface reflections and losses due to spreading and absorption. The sound speed depth profile is determined by the vertical variation of salinity, temperature and pressure. Bottom reflection losses are dependent on the nature of the bottom sediment, surface roughness and topography. Surface reflection losses are functions of ray grazing angle and the roughness of the ice cover. Absorption losses are due to the internal generation of heat as sound propagates. All the reflection and absorption losses are very much dependent on the frequency of propagation.

In the Arctic it is known that below the upper layer of several hundred feet the sound speed gradient with respect to the depth is fairly uniform and moderate. In addition, measurement data tend to indicate that spatial variation of such vertical sound speed profiles are small, especially in the central Arctic region. Under these conditions ray theory affords a very convenient and effective technique for calculating the acoustic intensities, ruling out those cases in which extreme low frequencies are considered (Section 2.2).

A typical ray diagram and sound speed profile using recent temperature and salinity data at Base Camp Station (72-0.20N latitude and 211-24.8 longitude) are plotted and presented in Section 6. The units of depth and range are in feet and the speed of sound in feet per second. The source is located 1000 feet below the surface and the initial grazing angles of the rays have one degree increment.

Such ray diagrams form the basis of calculating the acoustic intensities by ray theory. A program has been developed that is designed specifically for such sound intensity calculations at a given number of receiver stations corresponding to a given number of sources. The locations of the receiver stations and sources are specified in terms of latitude, longitude, and depth. Input parameters to the program are the frequency of propagation, typical salinity and temperature profiles, bottom topography and the RMS ice roughness.

4.1 SOUND SPEED PROFILE CALCULATION

The sound speed is a function of the local salinity, temperature and pressure. In general it is calculated by the Wilson's formula (Reference 1):

$$v = 1449.14 + v_T + v_P + v_S + v_{STP} \tag{1}$$

where

$$v = 4.5721T - 4.4532X10^{-2}T^2 - 2.6045X10^{-4}T^3 + 7.9851X10^{-6}T^4$$

$$v_P = 1.60272X10^{-1}P + 1.0268X10^{-5}P^2 + 3.5216X10^{-9}P^3 - 3.3603X10^{-12}P^4$$

$$v_S = 1.39799(S-35) + 1.69202X10^{-3}(S-35)^2$$

$$v_{STP} = (S-35)(-1.1244X10^{-2}T + 7.7711X10^{-7}T^2 + 7.7016X10^{-5}P$$
$$- 1.2943X10^{-7}P^2 + 3.1580X10^{-8}PT + 1.5790X10^{-9}PT^2) +$$
$$P(-1.8607X10^{-4}T + 7.4812X10^{-6}T^2 + 4.5283X10^{-8}T^3) +$$
$$P^2(-2.5294X10^{-7}T + 1.8563X10^{-9}T^2) + P^3(-1.9646X10^{-10}T)$$

T is the temperature in degrees Centigrade,
P is the pressure in kg/cm^2 (absolute),
S is the salinity in °/oo, and
v is the sound speed in m/sec.

The pressure at any depth z may be calculated by Leroy's formula (Reference 2):

$$P = 1.04 + 0.102506(1 + 0.00528 \sin^2\phi)z + 2.524X10^{-7}z^2 \tag{2}$$

where

z is the depth in meters and
ϕ is the latitude in degrees.

Although the Wilson's formula is generally used for sound speed calculations, a shorter and simpler version, claimed to fit applicable Wilson's data better, is due to Leroy (Reference 3):

$$v = v_o + v_a + v_b + v_c + v_d \tag{3}$$

where

$$v_o = 1493.0 + 3(T-10) - 6X10^{-3}(T-10)^2 - 4X10^{-2}(T-18)^2$$
$$+ 1.2(S-35) - 10^{-2}(T-18)(S-35) + z/61$$
$$v_a = 10^{-1}\zeta^2 + 2X10^{-4}\zeta^2(T-18)^2 + 10^{-1}\zeta\phi/90$$
$$v_b = 2.6X10^{-4}(T-5)(T-25)T$$
$$v_c = -10^{-3}\zeta^2(\zeta-4)(\zeta-8)$$
$$v_d = 1.5X10^{-3}(S-35)(1-\zeta) + 3X10^{-6}T^2(T-30)(S-35)$$

T is the temperature in degrees Centigrade,
S is the salinity in °/oo,
ϕ is the latitude in degrees,
z is the depth in meters, and
ζ = z/1000, i.e., depth in km.

Leroy claims that not all data used in establishing Wilson's formula are realistic in view of the actual conditions to be expected in the natural sea waters of the world and uses what he considers a more representative data base to establish his formula.

To find the sound speed at a particular depth corresponding to the given data of salinity and temperature at various depths, one first calculates the salinity and temperature at the desired depth by *spline interpolation*. This ensures "smooth" salinity-depth and temperature-depth profiles through the given data points in the sense not only the first but also the second derivatives are continuous from interval to interval. From the interpolated values of salinity and temperature the sound speed is then calculated by either the Wilson's or Leroy's formula.

In order to compare Wilson's and Leroy's formulas sound speed has been calculated at different depths (using spline interpolation of salinity and temperature as described above) up to 12000 feet in depth (Base Camp Station data of salinity and temperature). The results indicate that differences in sound speed calculated by both methods are insignificant, being of the order of 1/10 of one percent at larger depth. It thus appears that Leroy's formula can indeed be used to advantage because of its relative simplicity.

4.2 BOTTOM TOPOGRAPHY

In order to give a fairly adequate description of the topography of the Arctic Ocean bottom, 4800 stored words are assigned for this purpose. This covers the rectangular area of which the center is the North Pole: the midpoints of the four sides have the following latitudes and longitudes: 70°N 0°, 75°N 90°, 70°N 180° and 75°N 270°. This rectangle is partitioned into 4800 squares by dividing the horizontal sides into 80 equal intervals and the vertical sides into 60 intervals. Each such square thus has a side equal to about 34.55 miles, and each stored word represents the average depth of the ocean bottom for this area.

Although a number of sources are available for the bathymetric data of the Arctic Ocean, it is finally decided to make use of the Arctic Bathymetric maps as compiled by the Canadian Hydrographic Service, 1966-1967, which furnish fairly detailed information. However, these maps cover only the two quadrants of the Arctic: latitude 72°N longitude 180°-270° and latitude 72°N longitude 270°-360°; viz., these areas on the side of Alaska, Canada and Greenland. Fortunately much information can also be derived from the North Polar Chart compiled by the Hydrographic Department of the British Navy, 1969, which supplies the detailed bathymetric data on the Russian and European side.

A bathymetric computer plot showing the approximate depth of the Arctic Ocean bottom at 4800 locations is given in Section 6. As noted above, each letter or numeral represents the average depth of an area of about 34.55 mile square.

In order to give a visual description of the bottom topography, a number of Arctic Ocean contour plots are presented in Section 6, based on the stored depth data and plotted by CALCOMP. These plots give the various depth contours of 100, 300, 500, 700, 900 ft.; 1000, 2000, 3000, 4000, 5000 ft.; 6000, 7000, 8000, 9000, 10000 ft. and finally 11000, 12000, 13000, 14000, 15000 ft. In each of these plots the shore lines are also included. Although not explicitly indicated in these plots, the Lomonosov Ridge, the Canadian Abyssal Plain, the Amundsen Basin, the Fletcher Plain, etc., are distinctly visible.

4.3 RMS ICE ROUGHNESS

While it is possible to determine the RMS ice roughness from statistical considerations of the ice ridge spacings, sail heights and keel depths (Section 3.4), the acoustic experiments of Mellen and Marsh (Reference 4) and Kutschale (Reference 5) directly relate the ridge index (number of ridge counts per 30 nautical miles) with the RMS ice roughness. These experiments indicate the following relationship:

Ridge Index	RMS Ice Roughness
300 - 600	2.5 meters
600 - 900	3.0
900 - 1200	4.0

The results of computation in this report are based on the ridge index data in the spring season supplied by Whittmann and Schule (Reference 6). A plot of RMS ice roughness utilizing the above relationship is presented in Section 6.

4.4 ICE REFLECTION LOSS

It is reasonable to assume that for grazing angles less than 30°, little energy is lost through penetration into ice. For long range propagation only those rays that have perfect reflection at the underice surface have significant contribution to the acoustic intensities. Marsh (Reference 7) has shown that the loss per such reflection can be calculated by the following equation:

$$\alpha = -10 \log_{10}(1 - 2.57X10^{-4} f^{3/2} h^{8/5} \sin\theta) \qquad (4)$$

where α is the loss in db per reflection,
f is the frequency in hz.,
h is the RMS ice roughness in meters and
θ is the grazing angle at incidence of limiting ray.

As can be seen from (4), the reflection loss increases rapidly with frequency.

4.5 ABSORPTION LOSS

This is the loss due to the conversion of acoustic energy into heat when sound propagates in a medium. It can be calculated according to the formula suggested by Marsh and Schulkin (Reference 8):

$$\beta = \left(\frac{ASf_T f^2}{f_T^2 + f^2} + \frac{Bf^2}{f_T^2} \right) (1 - 6.54X10^{-4}P)(7.943X10^{-3}) \qquad (5)$$

where β is the absorption loss coefficient in db per kyd,

$A = 2.34X10^{-6}$, constant for ionic relaxation in sea water,

$B = 3.38X10^{-6}$, constant associated with pure water viscosity mechanism,

S is the salinity in °/oo,

P is the pressure in kg/cm^2,

T is the temperature in degree Centigrade,

f is the acoustic frequency in kcps, and

$f_T = 2.19X10^{(6-1520/(T+273))}$, the temperature dependent relaxation frequency in kcps at atmospheric pressure.

For the low frequency under consideration, viz., 20 hz., the above formula has to be extrapolated. An alternate formula for calculating the absorption loss coefficient is due to Thorp (Reference 9):

$$\beta = \frac{0.1f^2}{1 + f^2} + \frac{40f^2}{4100 + f^2} \qquad (6)$$

Formula (6) is obtained by fitting curves to actual measured data of low frequencies. For the same f (6) gives much higher values of β than those extrapolated by using (5). For example, for f = .020(20hz.), S = 34, T = 0°c, $\beta = 4.3886X10^{-5}$ db/kyd as calculated by (6) and $\beta = 4.29698X10^{-11}$ db/kyd by (5). But even using the larger value of β, the transmission loss is only 0.048 db for sound travel of 1000 km. The absorption loss is therefore insignificant for the low frequency under consideration.

Formula (5) is used in the program and throughout all computations. However, in view of the large discrepencies between the results calculated by (5) and (6), further work remains to done in this area when transmission of higher frequencies is considered.

4.6 BOTTOM REFLECTION LOSS

A detailed computation of the bottom reflection loss has not been carried out for the following reasons:

(a) The bottom reflection loss is a function of the grazing angle, the frequency of propagation, surface roughness and the nature of the bottom sediment. Data on the latter are very scarce.

(b) For long range propagation those rays that "bounce" many times on the bottom before reaching the receiver will suffer enough attenuation and their contribution to the sound intensity is insignificant compared with those rays that reach the receiver without touching the bottom.

(c) To trace each ray from the source to the receiver over the bottom topography, which is, at best, some approximation, requires enormous amount of computing time.

It therefore stands to reason, at least for a preliminary study, to consider only those rays which travel in a *uniform* channel bounded by the surface and an artificial flat bottom of some *effective depth*. Those rays which penetrate deeper than the effective depth are excluded from consideration.

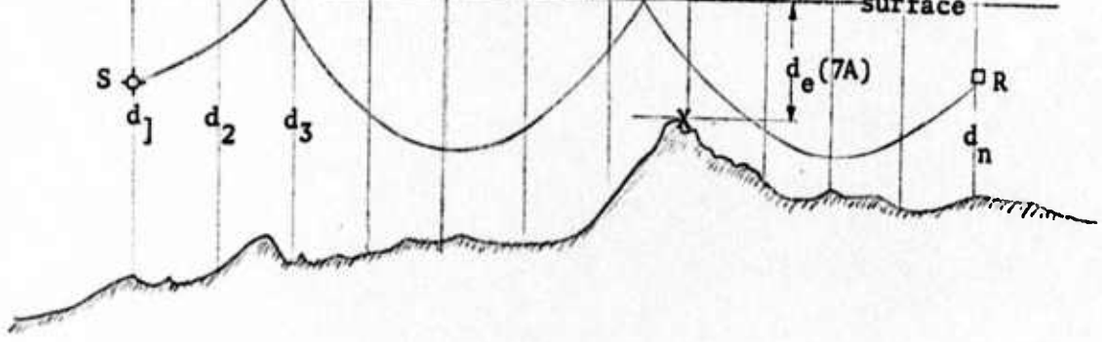

Fig. 1

To determine the effective depth d_e from source S to receiver R one finds the successive depths d_1, d_2, ---, d_n from the stored depth data by tracing a ray from S to R. Then d_e can be calculated in one of the following ways:

$$d_e = \min (d_1, d_2, ---, d_n) \tag{7A}$$

$$\frac{1}{d_e^2} = \frac{1}{n}\left(\frac{1}{d_1^2} + \frac{1}{d_2^2} + ---+ \frac{1}{d_n^2}\right) \tag{7B}$$

As shown in the figure d_e occurs at X based on (7A) but some rays can still travel from S to R without touching the bottom. Eq. (7B) is probably more realistic because it is the RMS of the reciprocals of the depths and gives emphasis to the minimum depth. This is the formula used in all the computations to determine an arbitrary bottom of the sound propagation channel.

Since the maximum grazing angle at the ice cover is limited to 30° (Section 4.4), and since, by assumption, those rays penetrate below the effective depth do not contribute to the acoustic intensity at the receiver, all the rays to be traced are enclosed between the two extreme rays making the apex angle $\Delta\theta$ at source S as shown.

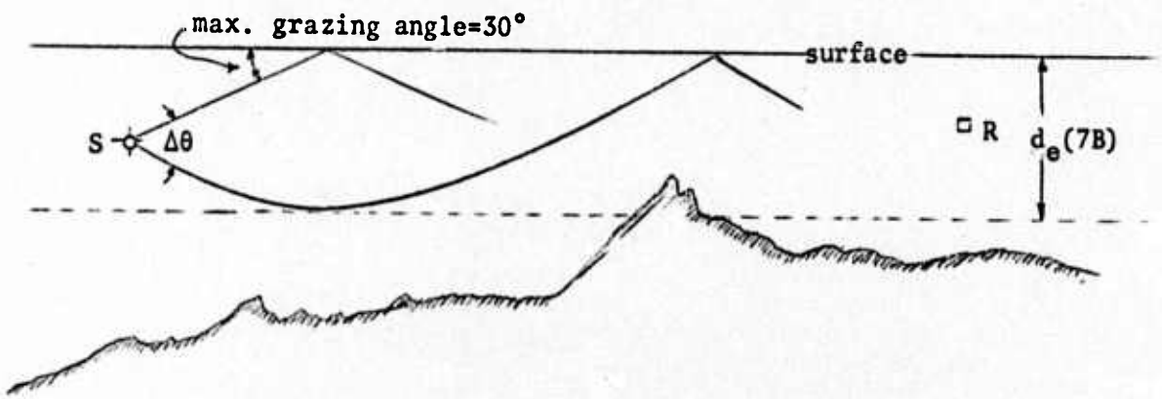

Fig. 2

4.7 STATISTICAL SUMMATION OF RAY INTENSITIES

The intensity I of each ray at range L from the source is given by:

$$I = -P \frac{\cos \theta}{L \frac{\partial L}{\partial \theta_o} \sin \theta} \qquad (8)$$

where I is the intensity in energy units per second per unit area,

P is the source strength in energy units per second,

θ_o is the initial grazing angle of the ray at the source, and

θ is the grazing angle of the ray at the point under consideration.

Thus to determine I for each ray an "adjacent" ray at grazing angle $\theta_o + \Delta\theta_o$ has to be traced simultaneously in order to evaluate $\partial L/\partial \theta_o$.

To calculate the acoustic intensity at receiver R at given range L from the source S, one should *theoretically* find all the rays from S that pass through R and sum up the intensities of the individual rays, taking into account the phase changes, etc. In view of the fact that the path of a ray is greatly dependent at any point of its travel on the speed of sound which is only approximately known, any slight variation in the speed of sound can cause the ray to deviate considerably from reaching the receiver R. Such a procedure is therefore only of academic interest, and the following one is used instead which is also computationally more efficient.

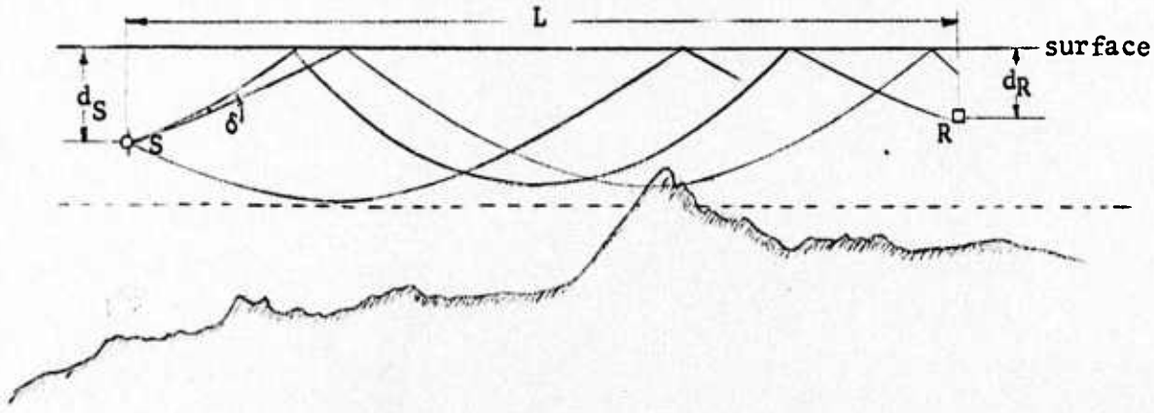

Fig. 3

We trace all the rays from S enclosed between the two extreme rays (Section 4.6) between the upper and lower boundaries with successive increment of δ in the initial grazing angles. Thus if N rays are traced, $\delta = \Delta\theta/N$.

Now at distance L from S, these rays will terminate at different depths d_i (i = 1, 2, ---,N), which are in general different from the depth of the receiver, d_R. However, because the speed of sound is only approximate, each ray has a chance of reaching R, and we assume that the probability of the ith ray to terminate at the receiver depends on the distance $|d_R-d_i|$ non-dimensionalized by d_e, the effective depth, i.e., $|d_R-d_i|/d_e$ and is given by the normal distribution:

$$\frac{1}{\sigma\sqrt{2\pi}} e^{-\frac{(d_R-d_i)^2}{2d_e^2\sigma^2}} \tag{9}$$

where σ is the standard deviation. If only a small number of rays are traced, obviously the bell shaped normal distribution should be flatter to include more rays at R, so it is reasonable to assume that σ depends on the number of rays traced: $\sigma = \kappa_1/\sqrt{N}$, κ_1 being an input parameter to the program (Reference 10). The average, or expected value of the intensity at R is therefore

$$\frac{1}{\sigma\sqrt{2\pi}} \Sigma I_i e^{-\frac{(d_R-d_i)^2}{2d_e^2\sigma^2}} \tag{10}$$

where I_i is the intensity of the ith ray at range L from S. Note that incoherent summation of the rays (phase neglected) is used here.

Since most measurement data are expressed in transmission loss (db), for purposes of comparison the corresponding transmission losses are computed according to the formula: $10 \log_{10}(I_o/I)$, where I_o is the intensity at 1 yard from the source.

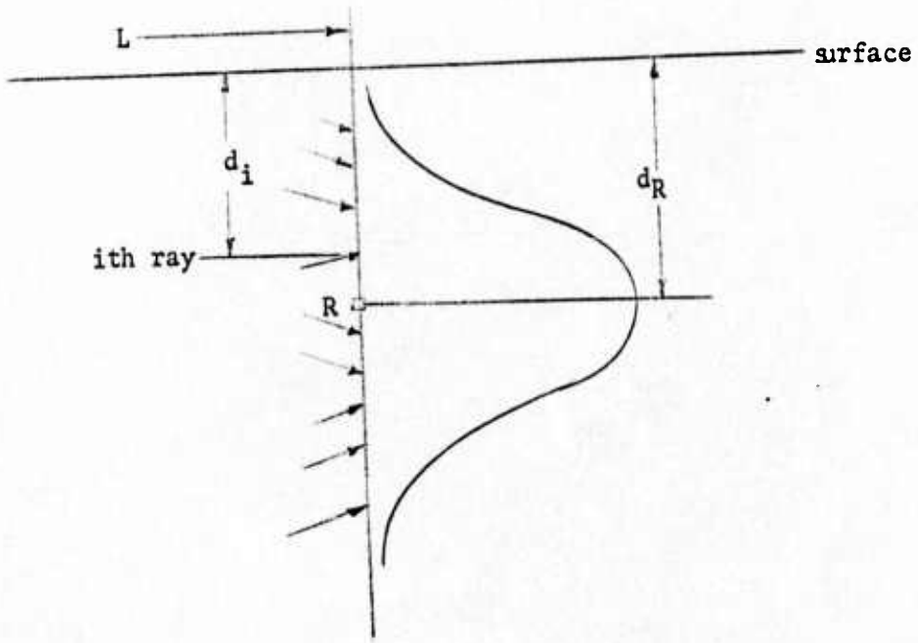

Fig. 4

4.8 CORRECTION FOR CAUSTICS

Abnormal high intensities of some of the rays may occur if for a given range from a source a position is reached which may be close to a caustic zone. Such a situation is likely to occur especially when a large number of rays are traced and will result in undue increase in the acoustic intensity when calculated by (10).

In order to correct this, the intensities of all rays traced are made to go through a filter to eliminate those values which markedly exceed the average value. The filtering device then detects these abnormal large values of $f_i = |I_i - I_A|/I_A$, where I_A is the arithmetic mean of I_i, $I_A = \Sigma I_i/N$, N being the total number of rays traced. Normally f_i should be less than 1; if $f_i > \kappa_2$, where κ_2 is an input parameter to the program (say $\kappa_2 = 2$), I_i will be considered to be close to a caustic and is simply rejected.

4.9 LLOYD MIRROR CORRECTION

For shallow sources or receivers the phase difference of the rays that arrive directly and by surface reflection will result in a modulation factor of the intensity given by $4 \sin^2((2\pi d/\lambda) \sin\theta)$, where d can be either the receiver depth or the source depth, λ the wave length and θ is the ray arriving grazing angle. This factor is applied to each individual ray traced, and is not taken into consideration (i.e., the factor is equal to 1) if d exceeds a certain depth, usually $\kappa_3\lambda$, where $\kappa_3<1$ and is an input parameter to the program.

4.10 ARCTIC PARTITIONING AND SOURCE AND RECEIVER LOCATIONS

The principal mountain ranges in Central Arctic are the Lomonosov Ridge and the Arctic Mid-Ocean Ridge, which run approximately in the direction of longitude 150°-330°. Between the ridges are the Amundsen Basin and the Pole Abyssal Plain. On the European side of the Arctic Mid-Ocean Ridge is the Nansen Basin and the Barents Plain; on the Alaska side of Lomonosov Ridge is the Markarov Basin and the Alpha Cordillera.

The sources and receivers are divided into five groups. The basis of the partitioning is that those receiver stations of one group can monitor sources of the same group much better than those sources belonging to a different group. This is because sources and receiver stations of different groups are usually separated by larger distances, and possibly by mountain ridges which partially obstruct ray propagation. Any movements in a deep channel can best be monitored by receivers in that channel.

Group I consists of seven sources and five receivers which are located in the sector with latitude less than 85° and longitude from 0° to 90°. This covers the shallow region of the Barents Sea, the Svyatata Anna Trough, part of the Nansen Basin and extends to the side of Greenland.

Group II consists of eight sources and six receivers covering the Arctic Mid-Ocean Ridge, the Amundsen Basin and the Lomonosov Ridge. In general this is the area of deep waters.

Group III consists of five sources and three receivers covering the shallow region of Laptev Sea and the deep Makarov Basin and the Fletcher Plain. It is a narrow strip which runs almost parallel to the Lomonosov Ridge.

Group IV consists of three sources and three receivers. The sources are scattered in the Alpha Cordillera and the receivers are close to Queen Elizabeth Islands.

Group V consists of four sources and three receivers and covers the East Siberian Sea, Chukchi Plateau and the Canada Abyssal Plain. The receivers are close to the shores of Alaska with receiver number 1 very near the Naval Arctic Research Laboratory at Point Barrow.

The latitude and longitude of the sources and receivers of the various groups are given in tabular form in Section 6. Also shown are the sources and receivers in the Arctic Ocean Contour Plots, page 67 - page 76.

4.11 COMPARISON OF COMPUTED RESULTS WITH FIELD MEASUREMENTS

For each partitioned group the acoustic intensity and transmission loss are computed for each receiver corresponding to each sound source. The receivers are placed at depths of 100, 200, 400, 600, 800, 1000, 1500, 2000, 3000 and 4000 feet; each source is located at depths of 20, 210, 410 and 610 feet. The detailed computed results are presented in Part II of this report. The range is the horizontal distance between the source and the receiver and the bottom level is the effective depth calculated according to Eq. (7B), Section 4.6, between the source and the receiver, both expressed in feet. The frequency of propagation is assumed to be 20 hz.

Extensive measurements of sound transmission loss in the Arctic have been carried out and reported by Marsh and Mellen (Reference 4) and also by Buck and Greene (Reference 11). These measured data of transmission loss against range are then combined and smooth curves are constructed which bestfit them at various frequencies. The smooth curves express the

relation between the transmission loss with range based on considerations of spreading and ice-water reflection loss (Reference 12). It is understood that in the experimental measurements, the receivers were at about 60 meters deep and the sources were at various depths up to 250 meters.

For receiver depth of 200 feet the computed transmission loss of *all* the cases considered is plotted against range irrespective of the bottom level. These plots are given in Section 6, page 77 - page 88. For each of these plots the sources are located at one of the depths: 20, 210, 410 or 610 feet. Thus the source and receiver depths correspond roughly to the conditions under which the experimental data were taken. For purposes of comparison the best-fit curve given by Buck (Reference 12) for 20 hz. is also included in each plot.

It is interesting to note that for shallow sources (20 feet below the surface) the calculated results all fall below the best-fit curve by Buck. The associated large transmission loss could be attributed to the Lloyd mirror effect. For sources 210 feet below the surface the calculated results are above the best-fit curve while for sources 410 and 610 feet below the surface, the calculated results again fall below this curve. Thus, on the average, the computed results agree quite well with experimental data.

4.12 COMPUTER PROGRAM

The ray tracing program is designed for the following purposes:

(a) From the given location of sources and receivers the program first finds the depth contours (depth values at regular intervals) from each source to each receiver, then calculates the effective depth according to (7B), Section 4.6.

(b) The program then calculates the acoustic intensity, and the transmission loss from each source to each of the receivers corresponding to the specified depths.

The program actually consists of two parts. From the input data the first part performs (a); the calculated depth data are combined with the input data and fed into the second part to perform (b).

The execution time depends greatly on the number of rays traced in each case. For tracing on the average of 90 rays from one source to one receiver, it takes about 160 seconds of CP time on the CDC 6600, or about 30 seconds of CP time on the CDC 7600. The core required is 65K with the depth data written on tape.

REFERENCES

1. Wilson, W. D., "Equation for the Speed of Sound in Sea Water," *The Journal of the Acoustical Society of America*, Vol. 32, No. 10, October, 1960.

2. Leroy, C. C., "Formulas for the Calculation of Underwater Pressure in Acoustics," *The Journal of the Acoustical Society of America*, Vol. 44, No. 2, August, 1968.

3. Leroy, C. C., "Development of Simple Equations for Accurate and More Realistic Calculation of the Speed of Sound in Sea Water," NATO TR No. 128, Saclant ASW Research Center, La Spegia, Italy, November, 1968.

4. Mellen, R. H. and Marsh, H. W., "Underwater Sound in the Arctic Ocean," AVCO Marine Electronics Office, New London, Connecticut, 1965.

5. Kutschale, H. W., "Arctic Hydroacoustics," *Arctic*, Vol. 22, No. 3, September, 1969.

6. Wittmann, W. and Schule, J. J., "Comments on the Mass Budget of Arctic Pack Ice," Naval Oceanographic Office, Washington, D. C., March, 1967.

7. Marsh, H. W., "Sound Reflection and Scattering from Sea Surface," *The Journal of the Acoustical Society of America*, Vol. 35, 1963.

8. Schulkin, M. and Marsh, H. W., "Sound Absorption in Sea Water," *The Journal of the Acoustical Society of America*, Vol. 34, No. 6, June, 1962.

9. Thorp, W. H., "Analytical Description of Low-frequency Attenuation Coefficient," *The Journal of the Acoustical Society of America*, Vol. 42, No. 1, July, 1967.

10. Davis, H., Fleming, H., Hardy, W. A., Miningham, R. and Rosenbaum, S., "Ray Tracing Program" Hudson Laboratory of Columbia University, Dobbs Ferry, N. Y., June, 1968.

11. Buck, B. M. and Greene, C. R., "Arctic Deep-water Propagation Measurements," *The Journal of the Acoustical Society of America*, Vol. 36, 1964.

12. Buck, B. M., "Arctic Acoustic Transmission Loss and Ambient Noise," *Arctic Drifting Stations*, Proceedings of the Symposium at Arctic Conference Center, Warrenton, Virginia, April, 1966, Sponsored by the Arctic Institute of North America.

5. SUBCONTRACT TO LAMONT-DOHERTY

The subcontract to Lamont-Doherty calls for the development of appropriate techniques to calculate the acoustic intensities in the Arctic Ocean, and comparisons of computed results by ray theory, normal mode theory, or any newly developed methods against experimental data. The principal effort is thus to search for a rapid, accurate method of computing propagation loss as a function of range in the ice covered Arctic Ocean. Important input parameters to the propagation model are ice roughness, bottom topography, and the velocity structure as a function of depth in the ice, water, and bottom sediments. Computational speed is of the utmost importance to evaluate variations of these parameters on propagation loss as a function of range since a number of models must be considered.

Such a rapid computational method is the Fast Field Program (FFP) technique discovered by Marsh (1967). The FFP was implemented for computation on a digital computer by Di Napoli (1971) for propagation in an all liquid wave guide. In the Arctic Ocean solid layers as well as liquid layers must be considered, and a convenient starting point for the FFP is the integral solution derived by matrix methods by Kutschale (1970, 1972) for propagation from point harmonic sources in a multilayered liquid-solid half space.

In the FFP technique the integral solution is evaluated rapidly as a function of range by numerical integration employing the Fast Fourier Transform (FFT). Singularities in the integrand corresponding to the normal mode poles are removed from the axis of integration by including an attenuation factor in each layer. The attenuation in each layer can represent the effects on propagation loss as a function of range of absorption of sound in the water, attenuation by the rough ice boundaries, and attenuation of sound by the bottom.

Two computer programs were written in Fortran IV to evaluate the liquid- and solid-bottom integral solutions derived by Kutschale (1970,1972). A comparison of the FFP computations with those computations by normal mode theory from the corresponding integral solutions are nearly identical, but the FFP technique is far more convenient and at least an order of magnitude

faster since the computations are done directly from the integral solution without first computing the roots of the frequency (period) equation and then summing the normal modes.

A number of comparisons of propagation loss computations have been made using ray theory (the program developed by Aerophysics Research Corporation), normal mode theory, and the numerical integration method developed by Lamont-Doherty. On page 89 are shown the computed propagation loss curves against range by various methods. Also included are the loss curves of Mellen and Marsh and of Buck (see References 4 and 12 of Section 4). These results indicate that for long range propagations the losses calculated by ray theory agree well with those by other methods.

Details of the numerical integration method are summarized in a separate report (Reference 5).

REFERENCES

1. Marsh, H. W. and Elam, S. R., Internal Document Raytheon Company, Marine Research Laboratory, New London, Connecticut, 1967.

2. DiNapoli, R. R., "Fast Field Program for Multilayered Media," Naval Underwater Systems Center Report No. 4103, 1971.

3. Kutschale, H. W., "The Integral Solution of the Sound Field in a Multilayered Liquid-Solid Half Space with Numerical Computations for Low Frequency Propagation in the Arctic Ocean," Lamont-Doherty Geological Observatory of Columbia University, Technical Report No. CU1-1-70, 1970.

4. Kutschale, H. W., "Further Investigation of the Integral Solution of the Sound Field in Multilayered Media; A Liquid-Solid Half Space with a Solid Bottom," Lamont-Doherty Geological Observatory of Columbia University Technical Report No. CU-6-71, 1972.

5. Kutschale, H. W., "Rapid Computation of Propagation Loss in the Arctic Ocean by Wave Theory," Lamont-Doherty Geological Observatory of Columbia University Technical Report, in Press.

6. COMPUTED RESULTS AND PLOTS

In this section we present the final computed results in graph form. The detailed output is reproduced in Part II of the report.

As has been mentioned elsewhere in the report, the frequency of propagation is 20 hz. The location of sources and receivers is given and plotted on page 67 - page 76. The typical temperature and salinity data are the recent measurement values taken at Base Camp Station (72°-02.0N latitude and 211°-24.8 longitude):

Depth (meters)	Temp. (°C)	Salinity (°/oo)
20	-1.59	29.822
26	-1.58	29.832
28	-1.60	29.829
30	-1.58	29.842
32	-1.58	29.905
34	-1.38	30.103
36	-1.28	30.208
38	-1.27	30.256
40	-1.24	30.346
60	-1.12	31.476
90	-1.33	32.298
120	-1.46	32.664
150	-1.47	32.902
180	-1.50	33.137
210	-1.32	33.526
240	-0.80	34.158
270	-0.33	34.486
350	0.25	34.758
500	0.49	34.856
650	0.33	34.875
800	0.12	34.883
1000	-0.08	34.898

RAY DIAGRAM (BASE CAMP DATA)

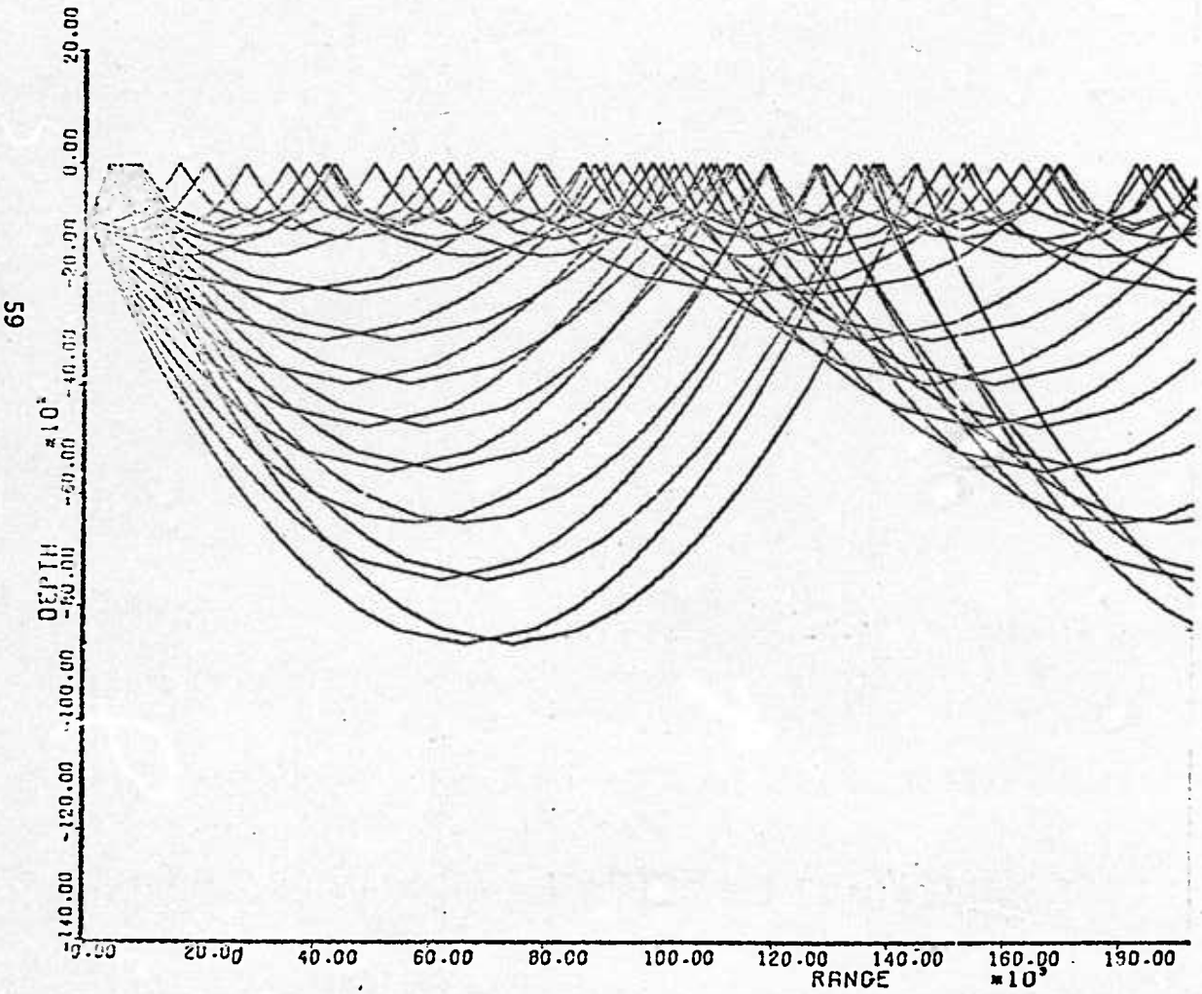

VELOCITY PROFILE

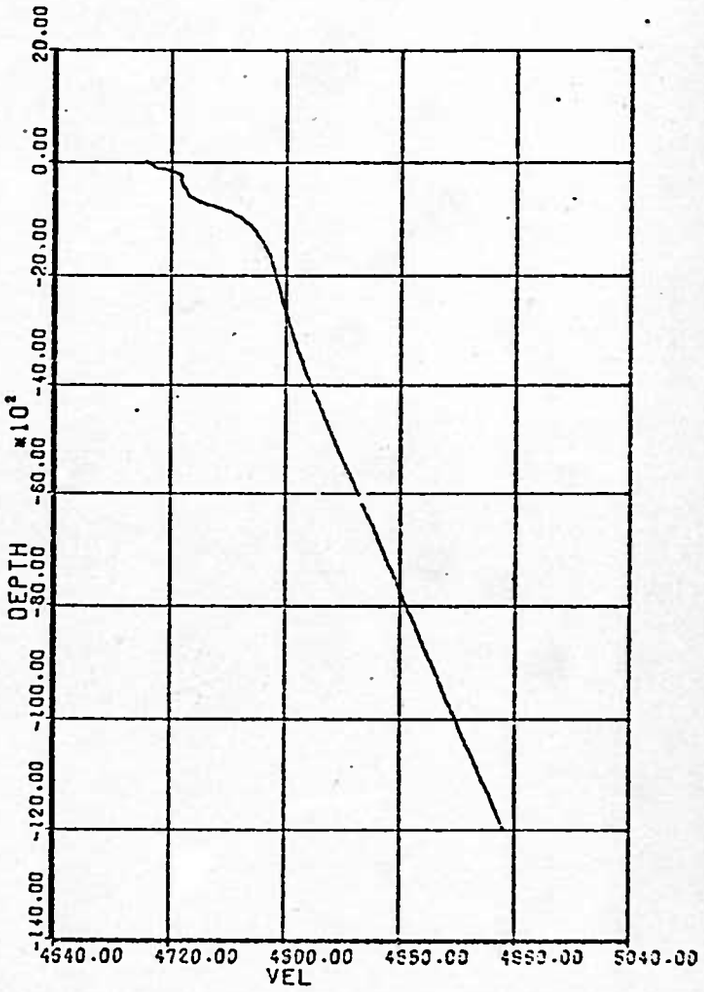

ARCTIC BATHOMETRIC PLOT

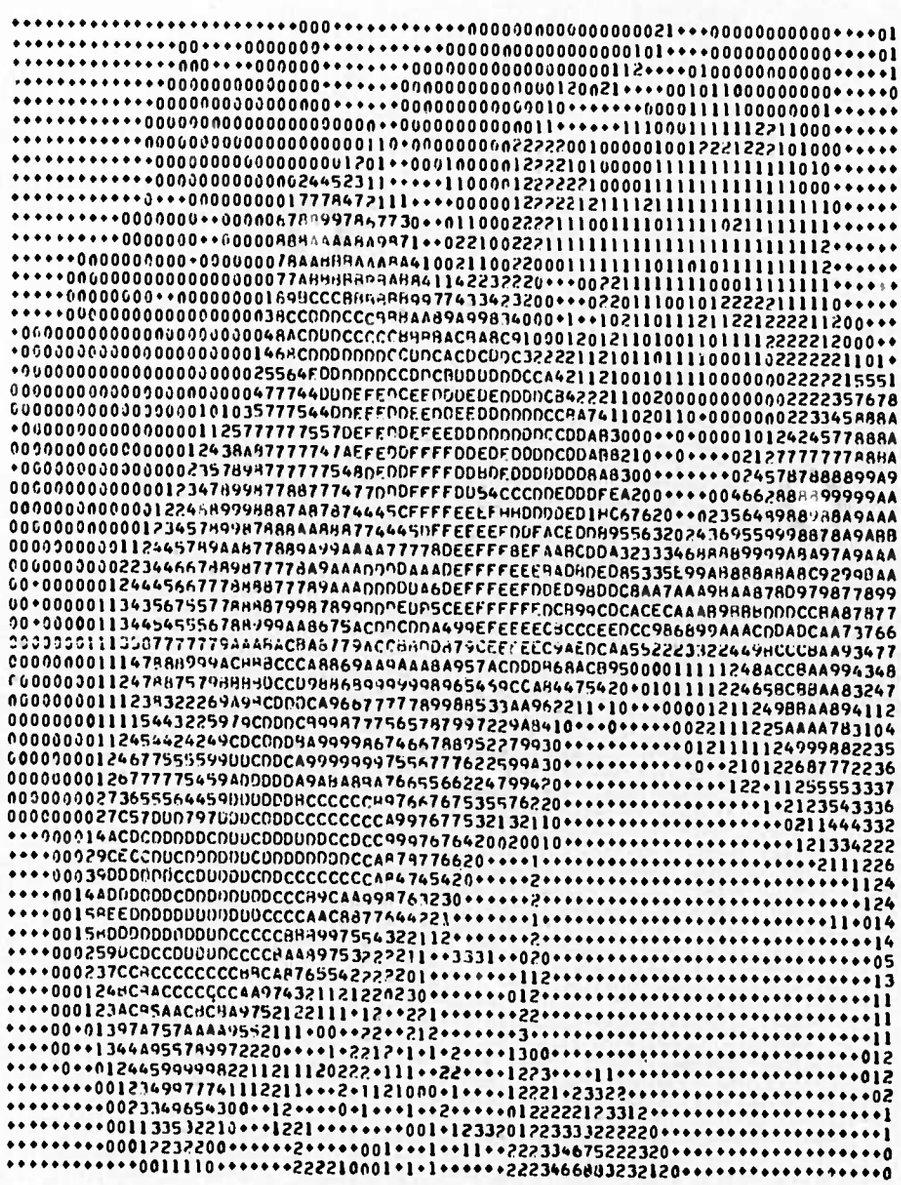

* INDICATES LAND. ALL NUMERALS AND LETTERS ARE DEPTHS

0= 0FT- 500FT	1= 501FT- 1000FT	2= 1001FT- 2000FT
3= 2001FT- 3000FT	4= 3001FT- 4000FT	5= 4001FT- 5000FT
6= 5001FT- 6000FT	7= 6001FT- 7000FT	8= 7001FT- 8000FT
9= 8001FT- 9000FT	A= 9001FT-10000FT	B=10001FT-11000FT
C=11001FT-12000FT	D=12001FT-13000FT	E=13001FT-14000FT
F=14001FT-15000FT	G=15001FT-16000FT	H=16001FT-17000FT
I=17001FT-18000FT		

ARCTIC OCEAN CONTOURS

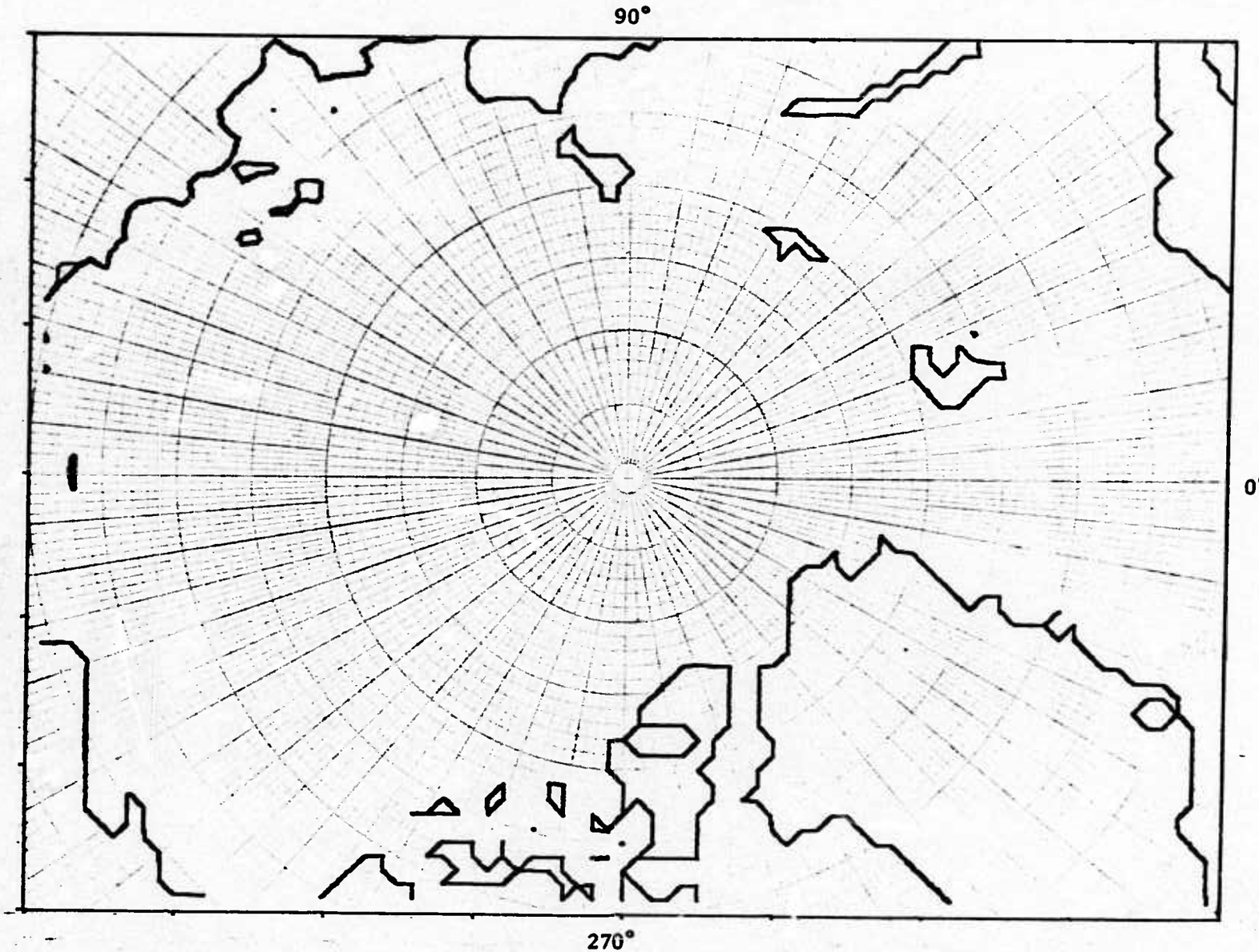

ARCTIC OCEAN CONTOURS

DEPTH CONTOURS OF 100, 300, 500, 700, 900 FT.

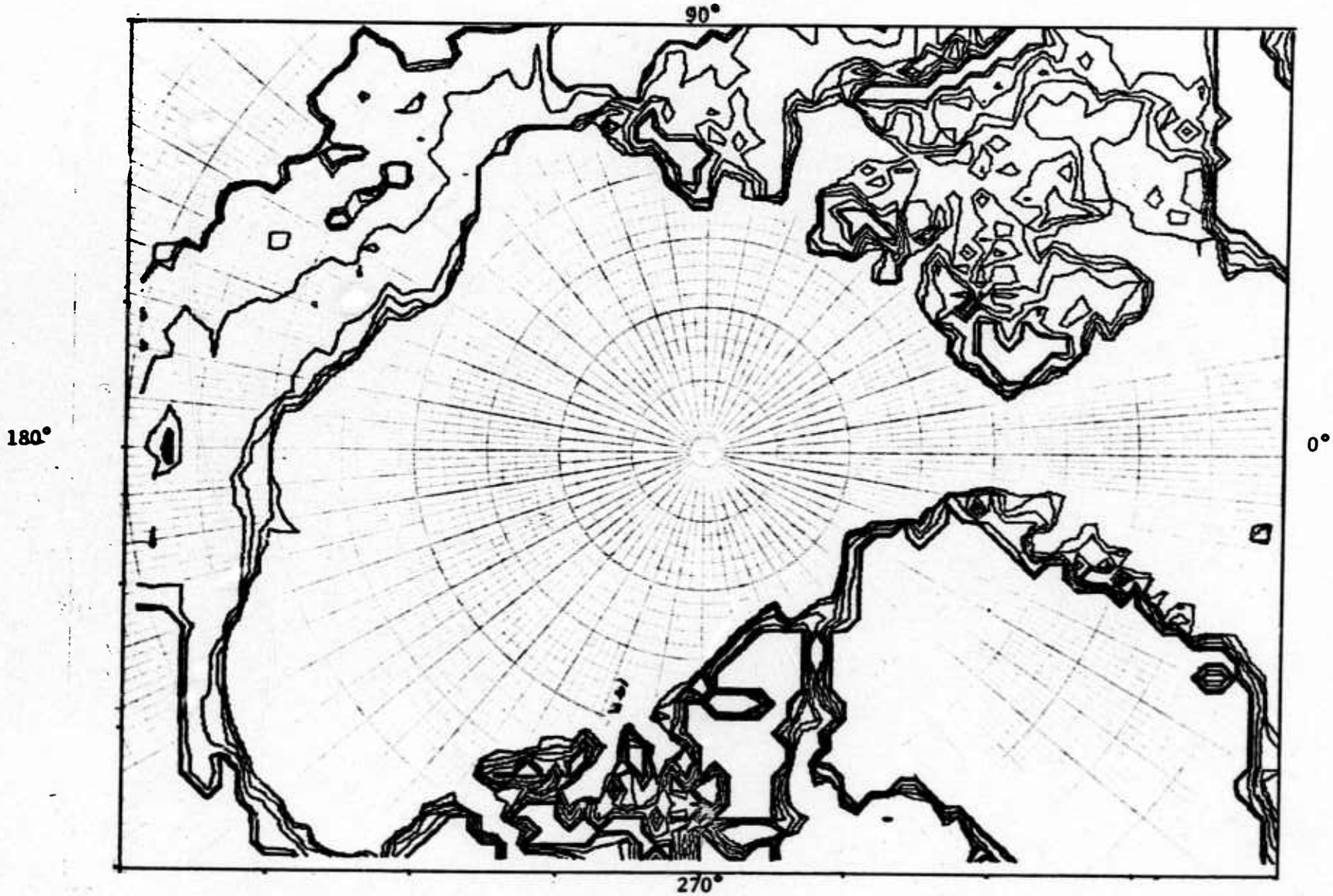

ARCTIC OCEAN CONTOURS

DEPTH CONTOURS OF 1000, 2000, 3000, 4000, 5000 FT.

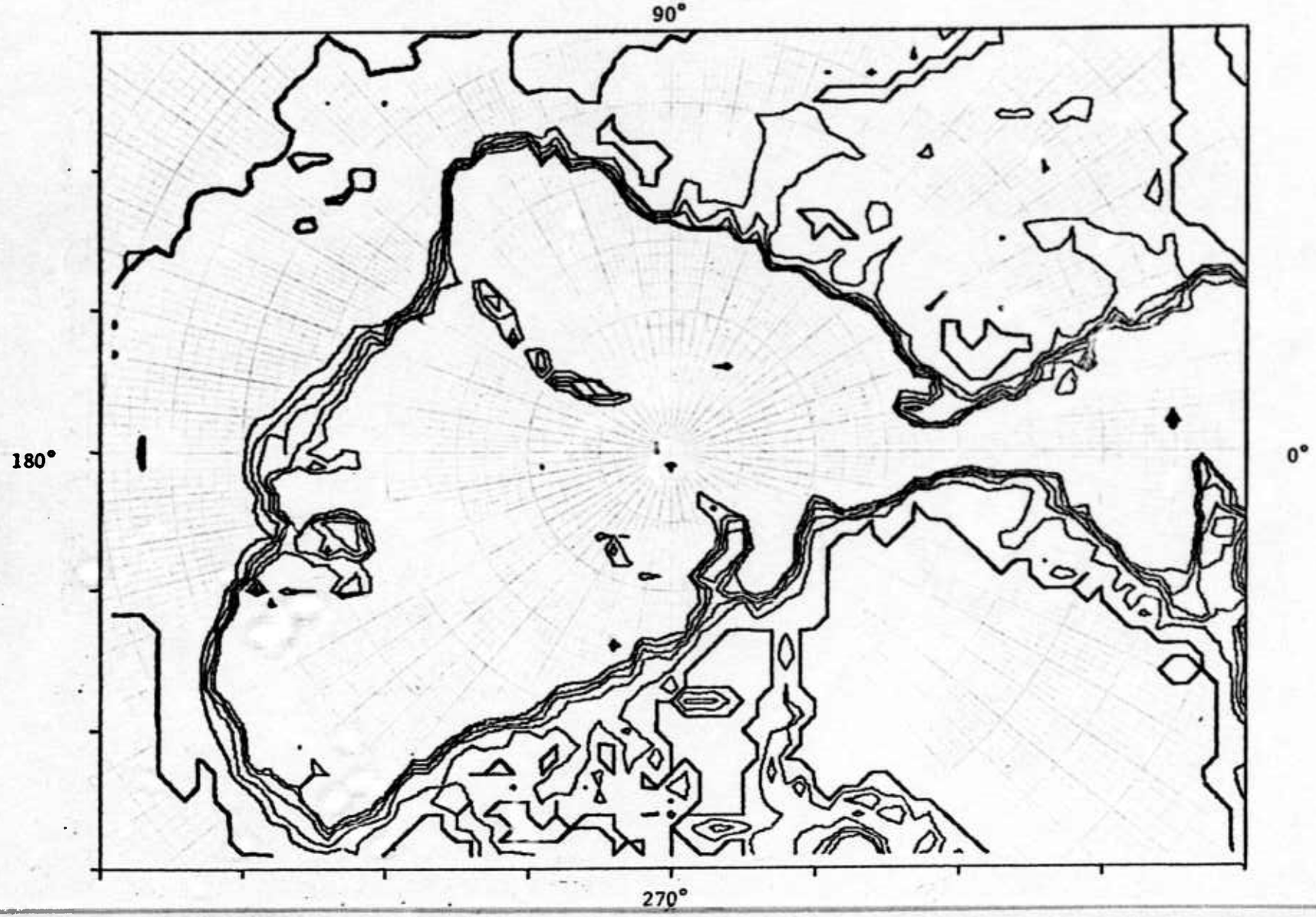

ARCTIC OCEAN CONTOURS

DEPTH CONTOURS OF 6000, 7000, 8000, 9000, 10000 FT.

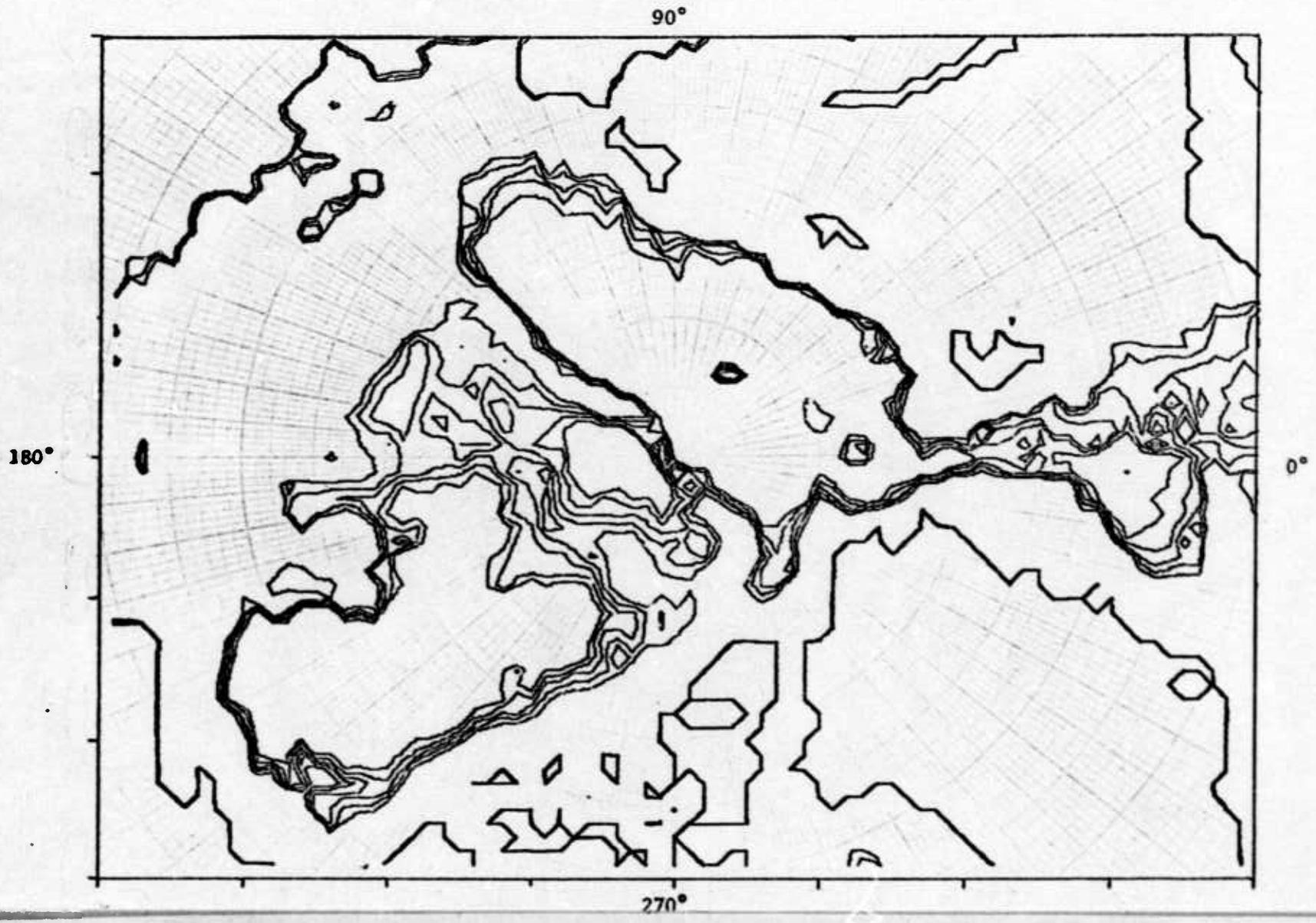

ARCTIC OCEAN CONTOURS

DEPTH CONTOURS OF 11000, 12000, 13000, 14000, 15000 FT.

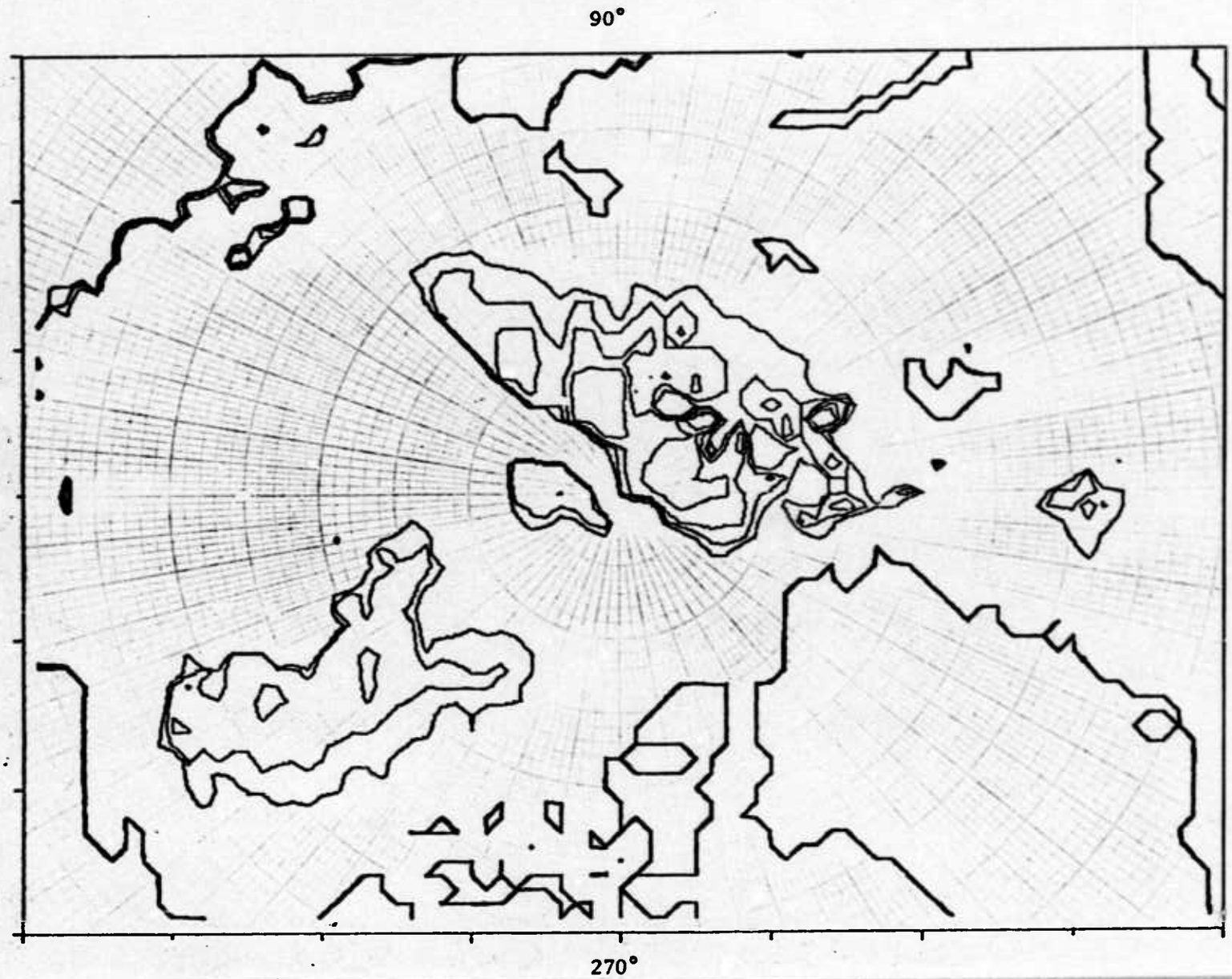

ICE ROUGHNESS CONTOURS

CONTOURS OF RMS ROUGHNESS IN METERS

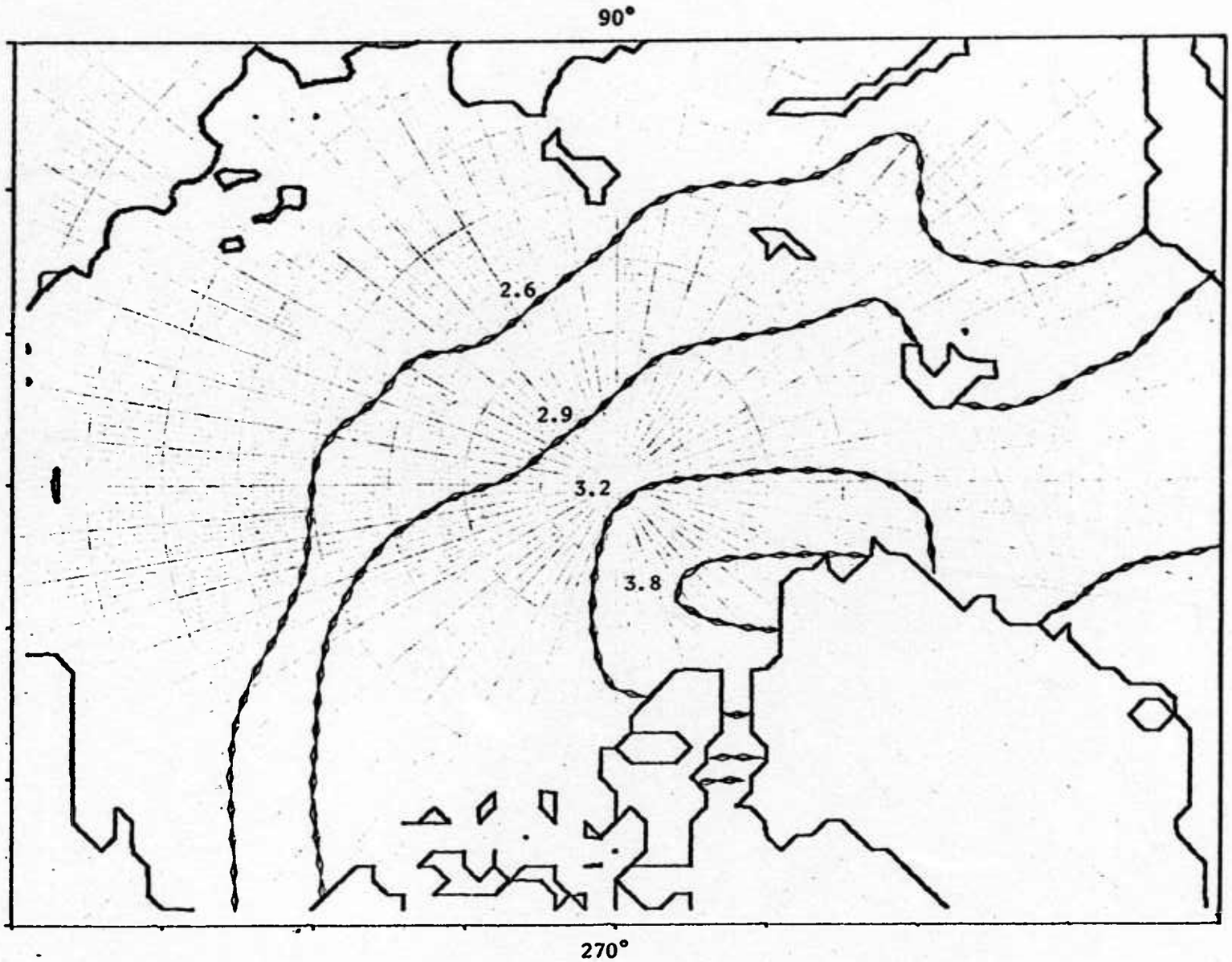

TABLE OF SOURCE AND RECEIVER LOCATIONS AND BOTTOM DEPTHS

GROUP I

		LONGITUDE	LATITUDE	BOTTOM DEPTH (FT.)
SOURCE	1	55.0	77.5	474
	2	39.0	73.0	990
	3	5.0	74.0	9600
	4	23.0	72.0	1080
	5	80.0	77.0	240
	6	80.0	83.5	12600
	7	40.0	84.0	12300
RECEIVER	1	35.0	78.0	468
	2	18.0	75.0	300
	3	75.0	81.5	3600
	4	350.0	76.0	3281
	5	34.0	81.5	10200

ARCTIC OCEAN CONTOURS

GROUP I 7 SOURCES AND 5 RECEIVERS

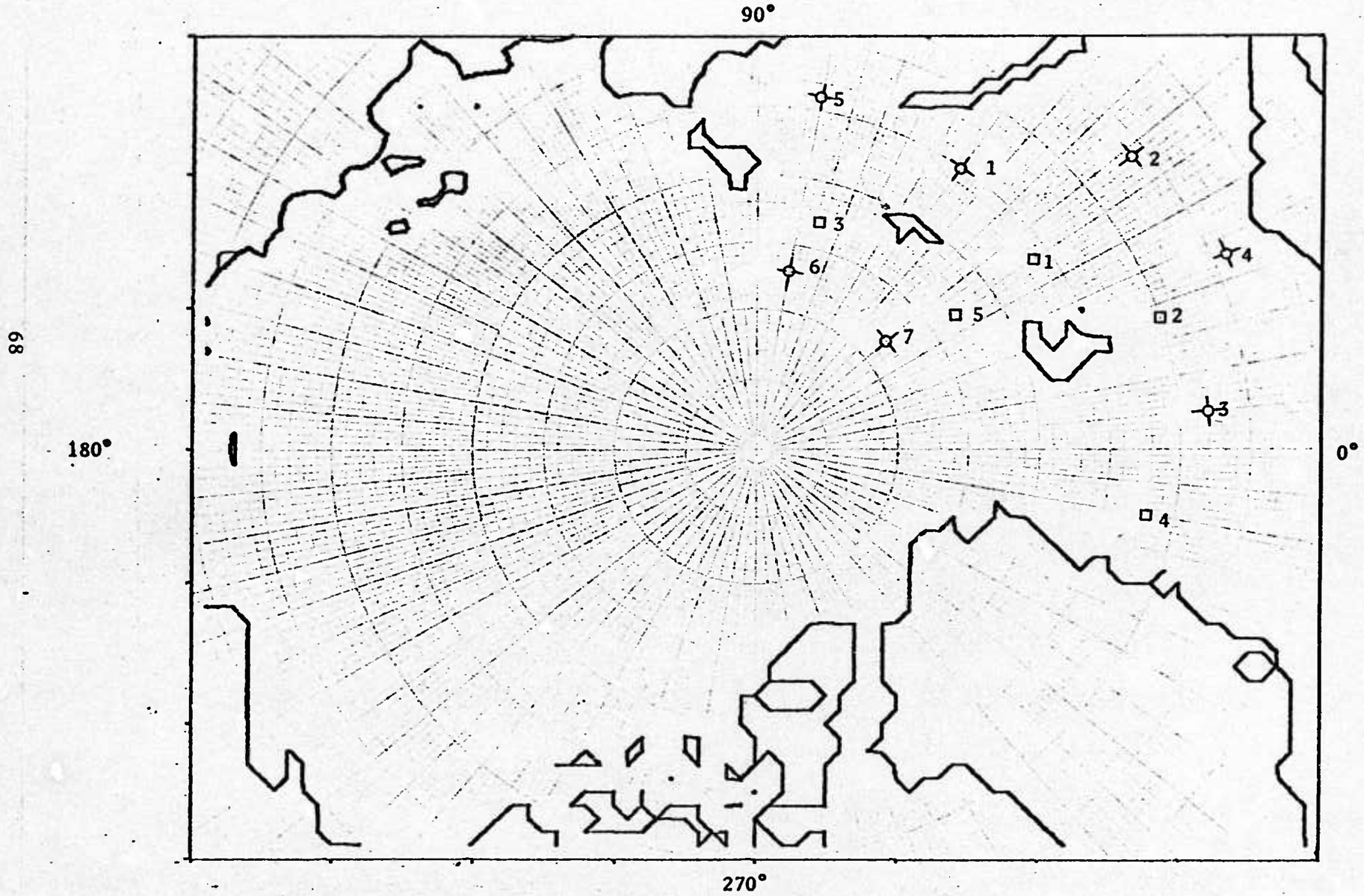

TABLE OF SOURCE AND RECEIVER LOCATIONS AND BOTTOM DEPTHS

GROUP II

		LONGITUDE	LATITUDE	BOTTOM DEPTH (FT.)
SOURCE	1	40.0	84.0	12300
	2	80.0	83.5	12600
	3	105.0	81.0	10200
	4	30.0	88.5	14400
	5	115.0	85.5	14400
	6	124.0	81.5	11400
	7	127.0	77.0	5400
	8	147.0	80.5	6000
RECEIVER	1	10.0	82.0	12600
	2	328.0	85.0	8202
	3	150.0	85.0	3000
	4	145.0	87.0	6000
	5	315.0	84.0	9514
	6	130.0	79.0	8400

ARCTIC OCEAN CONTOURS

GROUP II 8 SOURCES AND 6 RECEIVERS

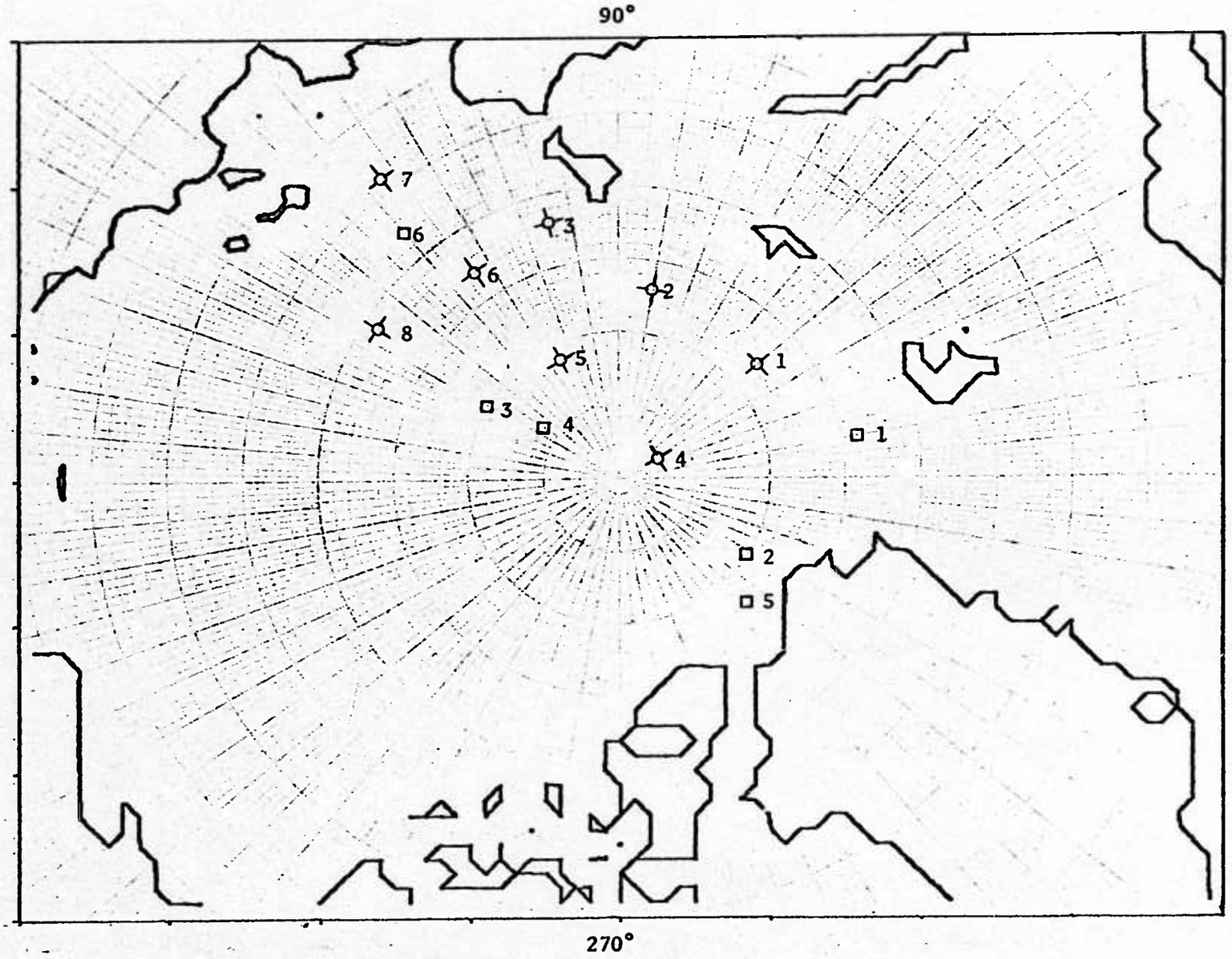

TABLE OF SOURCE AND RECEIVER LOCATIONS AND BOTTOM DEPTHS

GROUP III

		LONGITUDE	LATITUDE	BOTTOM DEPTH (FT.)
SOURCE	1	214.0	87.0	9186
	2	161.0	84.5	8400
	3	147.0	80.5	6000
	4	127.0	77.0	5400
	5	165.0	73.8	144
RECEIVER	1	272.0	85.0	5344
	2	160.0	81.0	6600
	3	250.0	85.7	5249

ARCTIC OCEAN CONTOURS

GROUP III 5 SOURCES AND 3 RECEIVERS

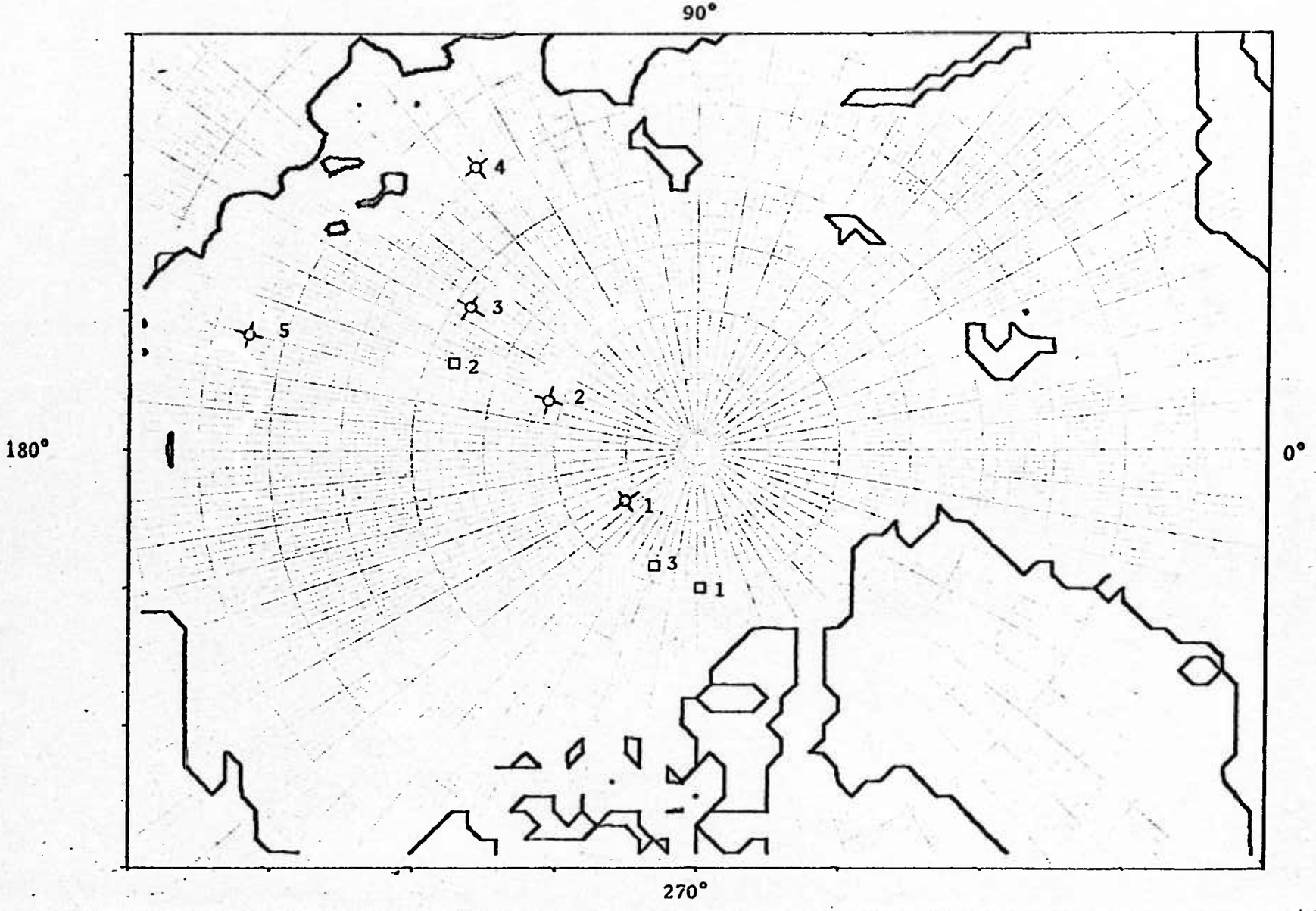

TABLE OF SOURCE AND RECEIVER LOCATIONS AND BOTTOM DEPTHS

GROUP IV

		LONGITUDE	LATITUDE	BOTTOM DEPTH (FT.)
SOURCE	1	223.0	82.5	11482
	2	190.0	82.0	9842
	3	168.0	79.5	8700
RECEIVER	1	250.0	81.0	6561
	2	237.0	77.0	984
	3	220.0	74.0	11483

ARCTIC OCEAN CONTOURS

GROUP IV 3 SOURCES AND 3 RECEIVERS

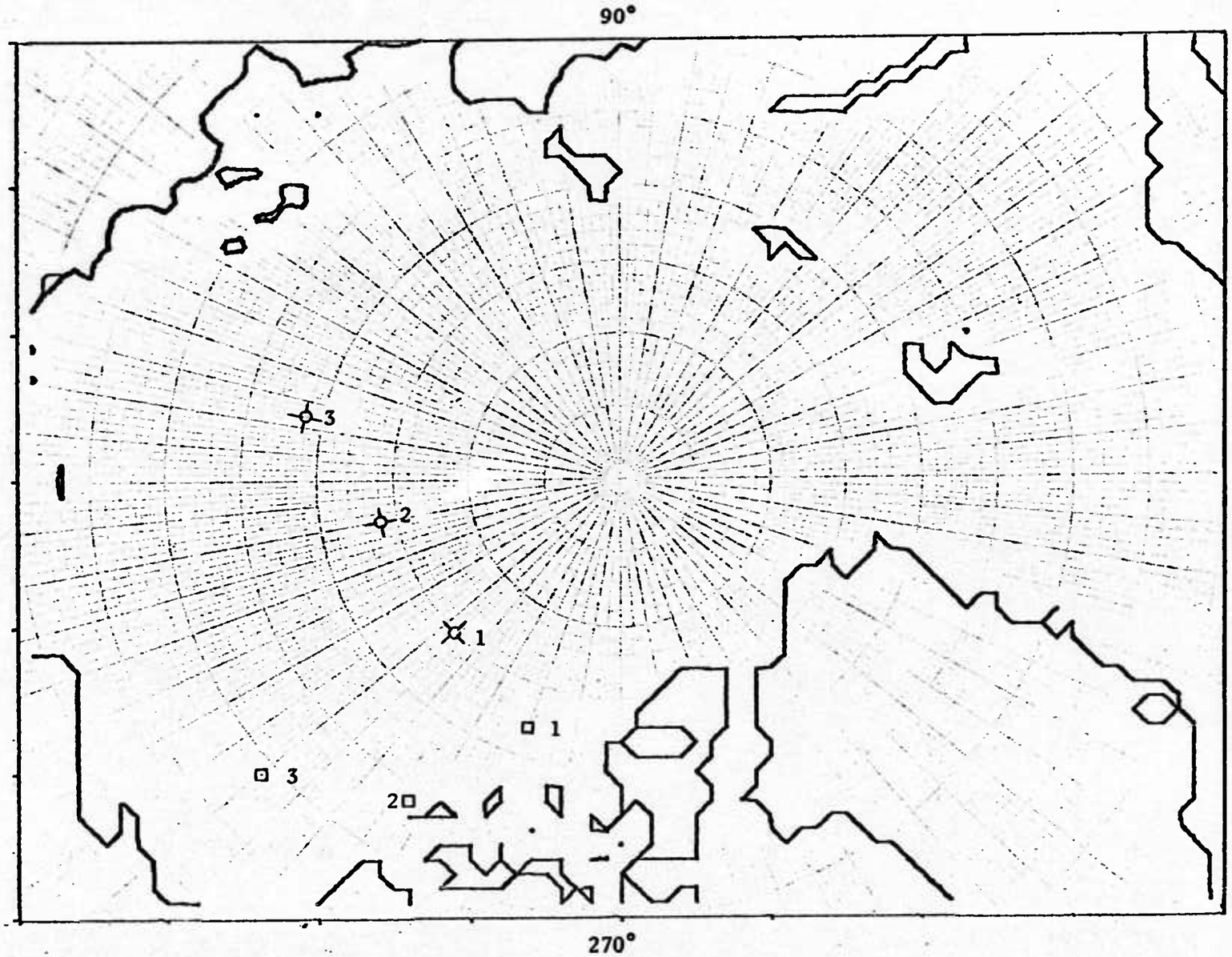

TABLE OF SOURCE AND RECEIVER LOCATIONS AND BOTTOM DEPTHS

GROUP V

		LONGITUDE	LATITUDE	BOTTOM DEPTH (FT.)
SOURCE	1	168.0	79.5	8700
	2	179.0	72.5	144
	3	165.0	73.8	144
	4	150.0	74.0	54
RECEIVER	1	205.0	72.5	8202
	2	195.0	78.0	1548
	3	190.0	70.0	131

ARCTIC OCEAN CONTOURS

GROUP V 4 SOURCES AND 3 RECEIVERS

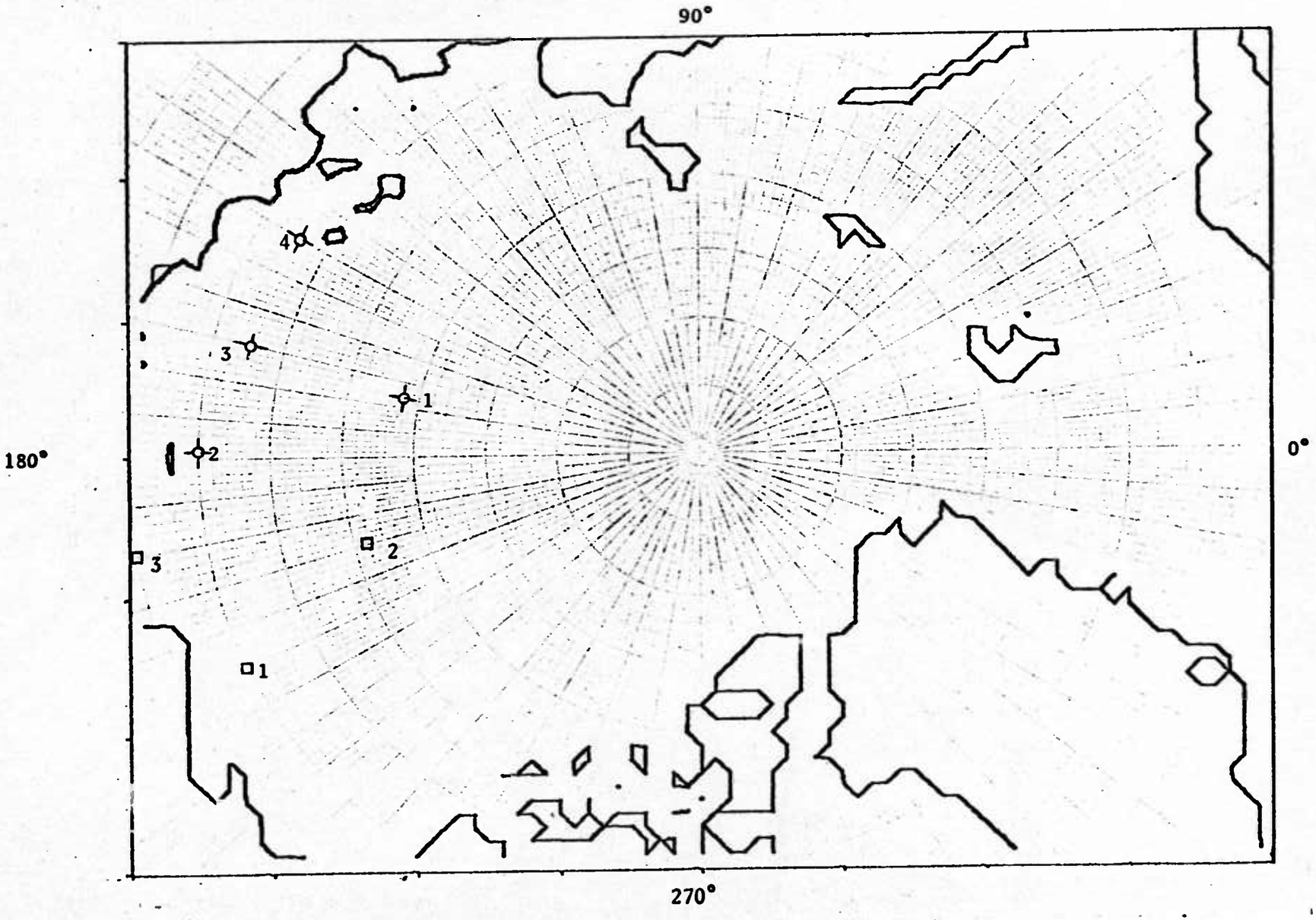

CALCULATED RESULTS AND BEST FIT CURVE FROM MEASUREMENTS (B. M. BUCK)

GROUP I o DEPTH OF SOURCES = 20 FT., DEPTH OF RECEIVERS = 200 FT.

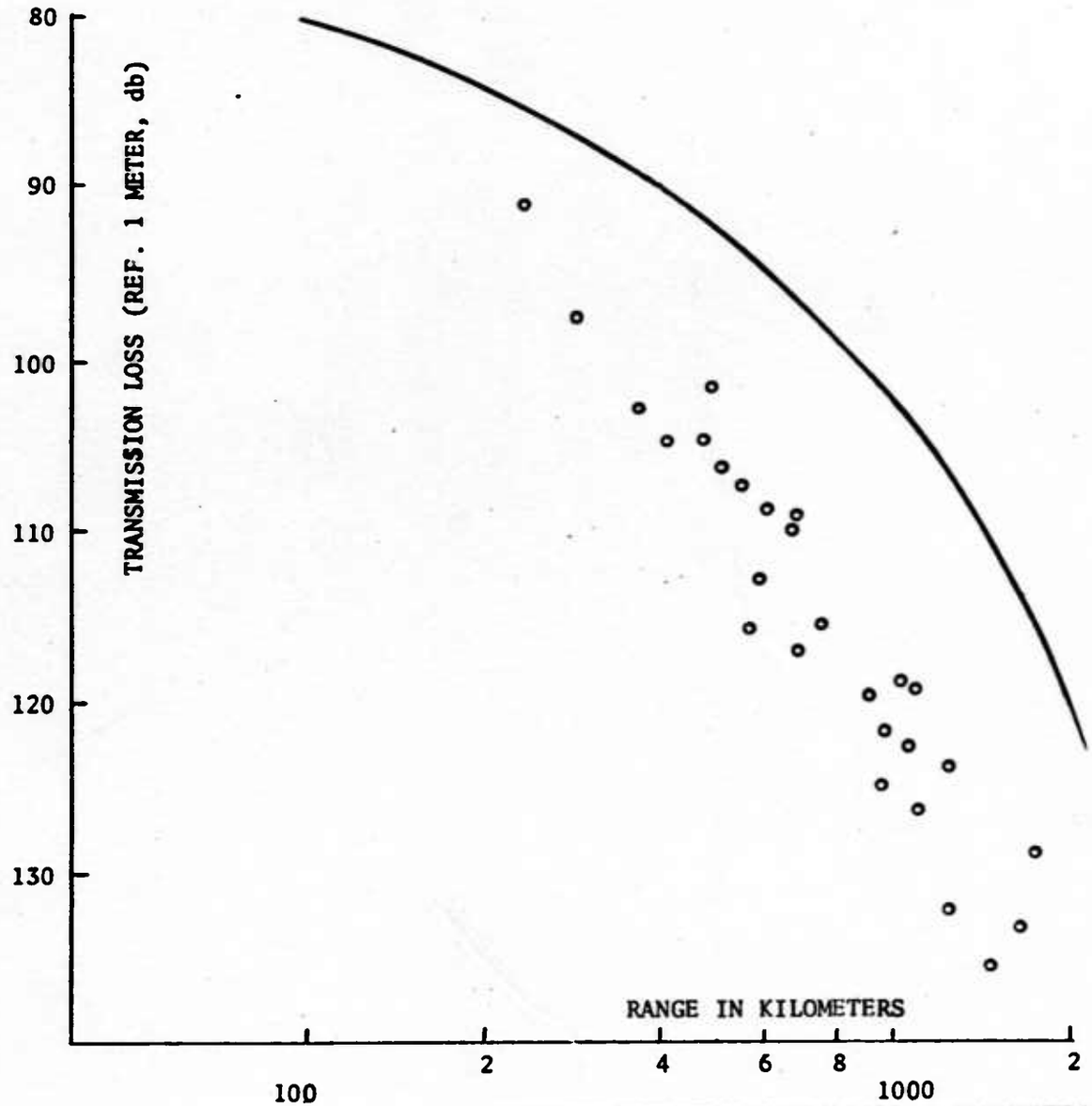

CALCULATED RESULTS AND BEST FIT CURVE FROM MEASUREMENTS (B. M. BUCK)

GROUP I o DEPTH OF SOURCES = 210 FT., DEPTH OF RECEIVERS = 200 FT.

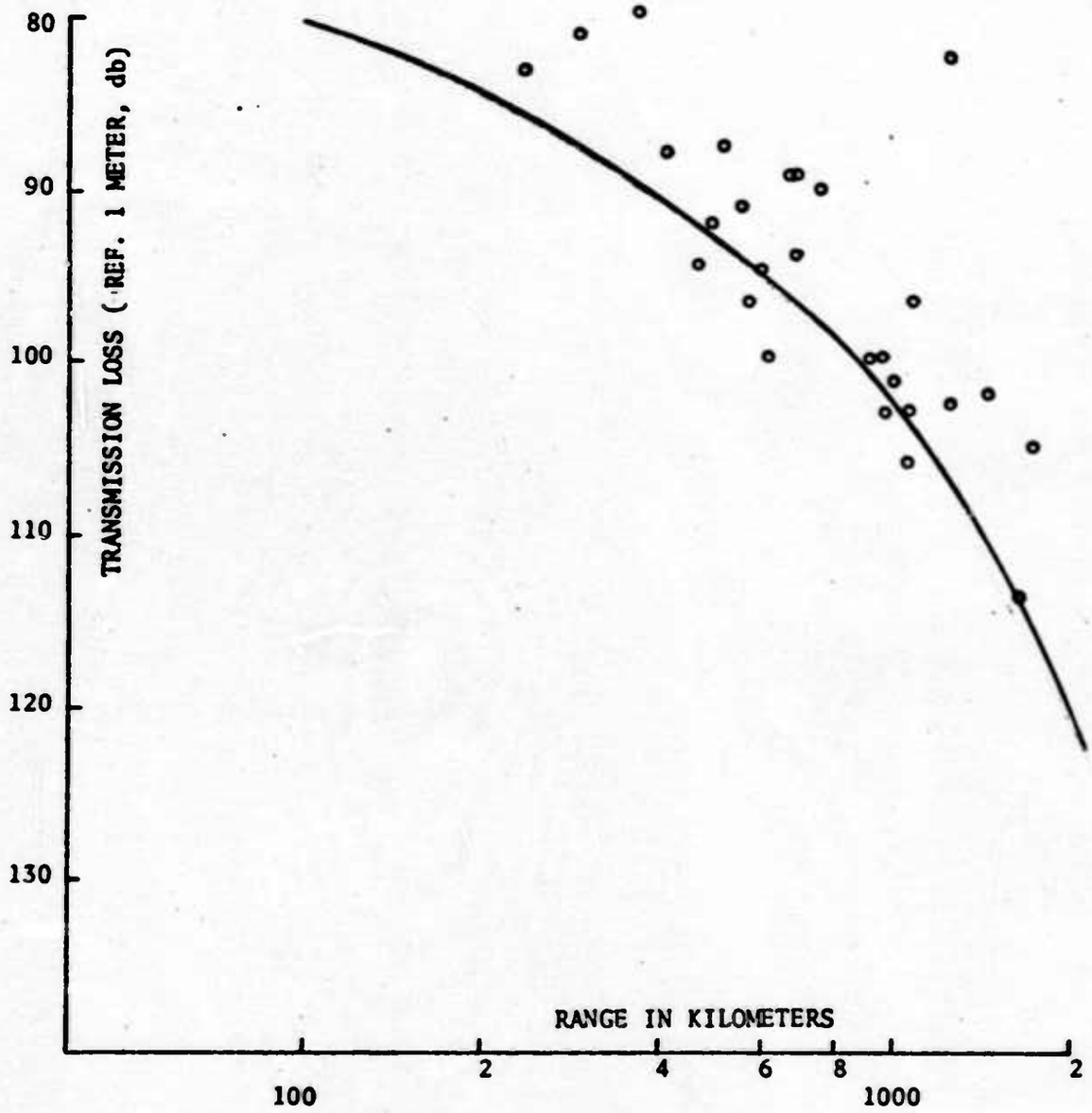

CALCULATED RESULTS AND BEST FIT CURVE FROM MEASUREMENTS (B. M. BUCK)

GROUP I o DEPTH OF SOURCES = 410 FT., DEPTH OF RECEIVERS = 200 FT.

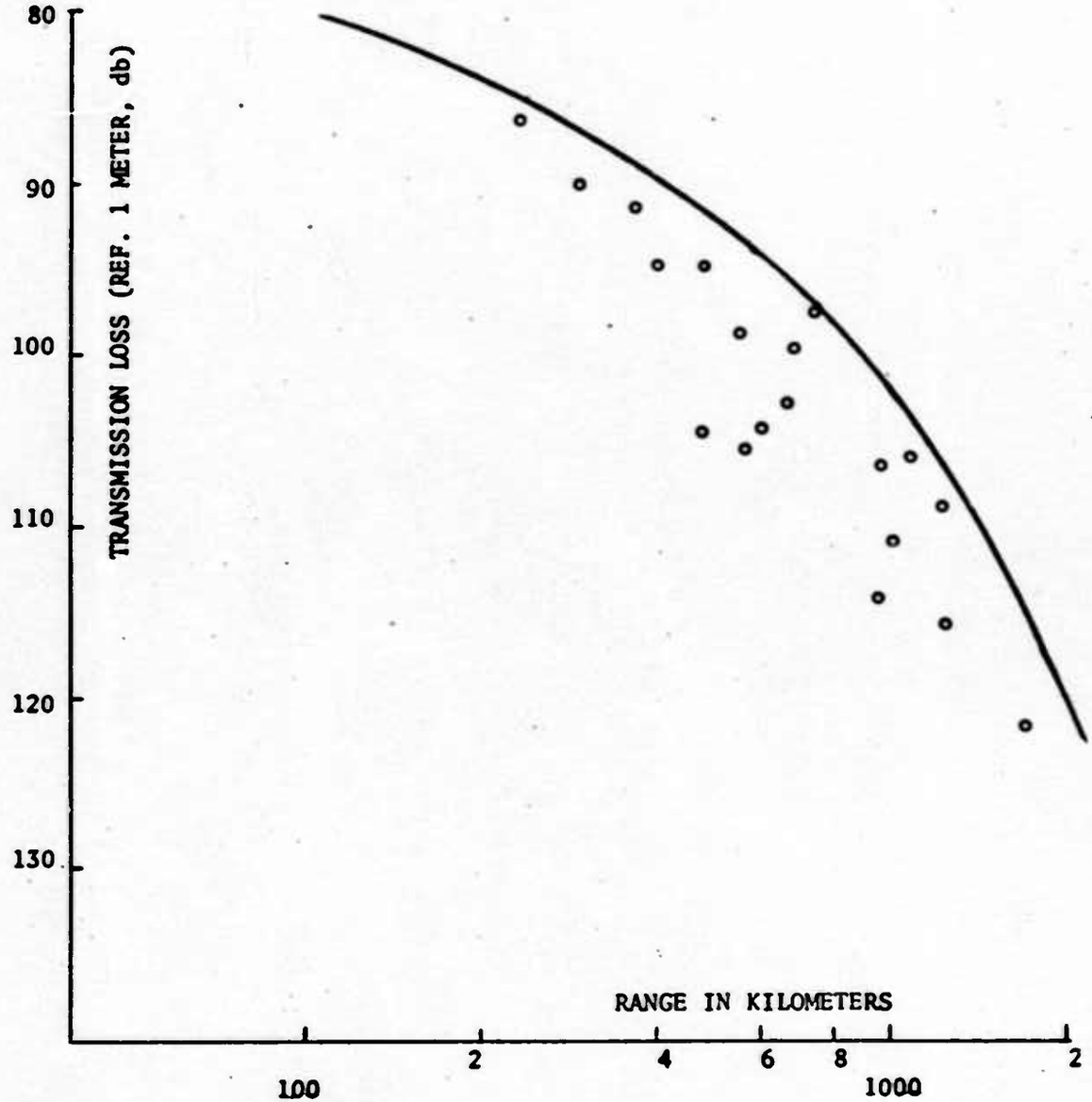

CALCULATED RESULTS AND BEST FIT CURVE FROM MEASUREMENTS (B. M. BUCK)

GROUP I ∘ DEPTH OF SOURCES = 610 FT., DEPTH OF RECEIVERS = 200 FT.

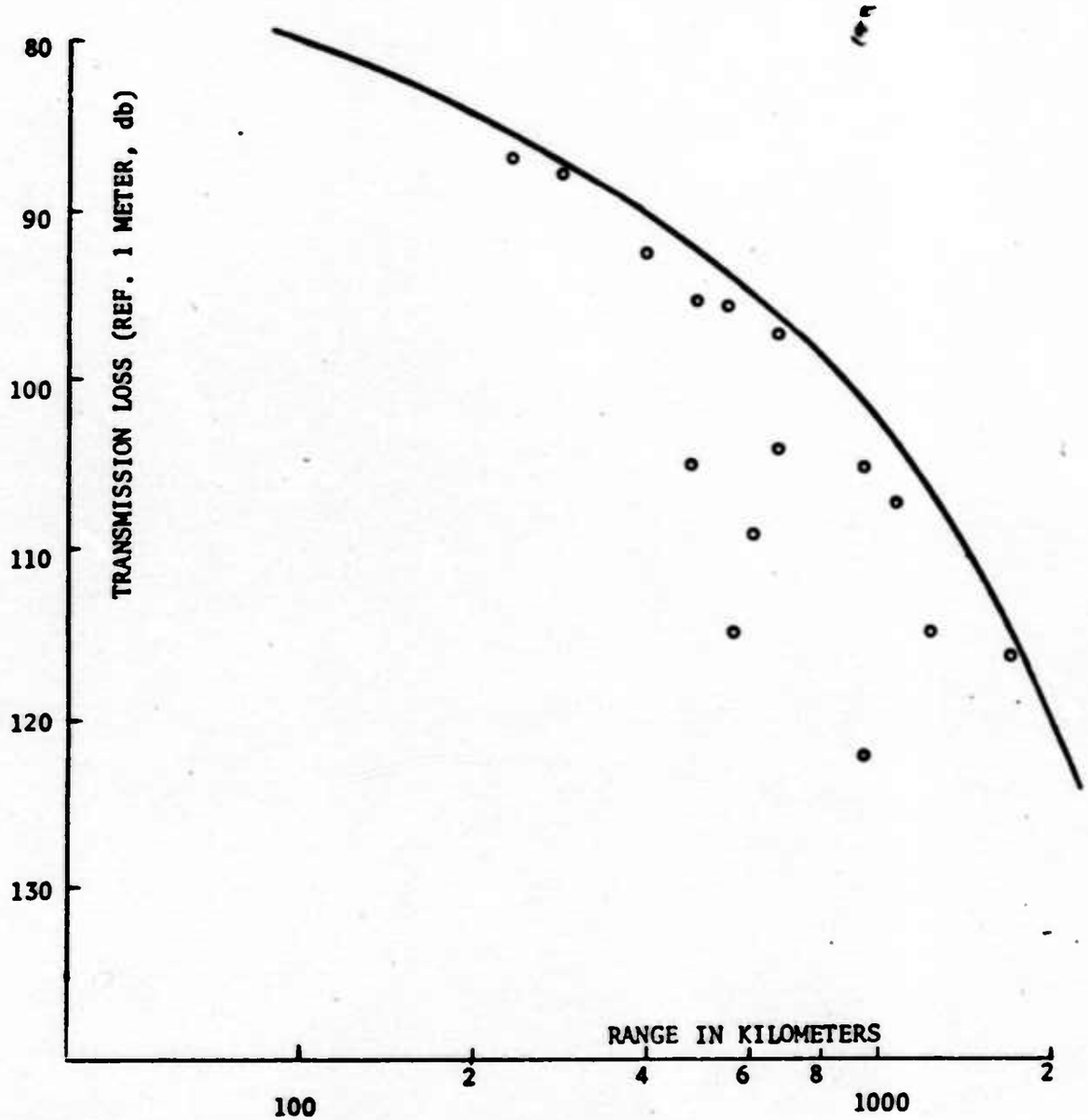

CALCULATED RESULTS AND BEST FIT CURVE FROM MEASUREMENTS (B. M. BUCK)

GROUP II o DEPTH OF SOURCES = 20 FT., DEPTH OF RECEIVERS = 200 FT.

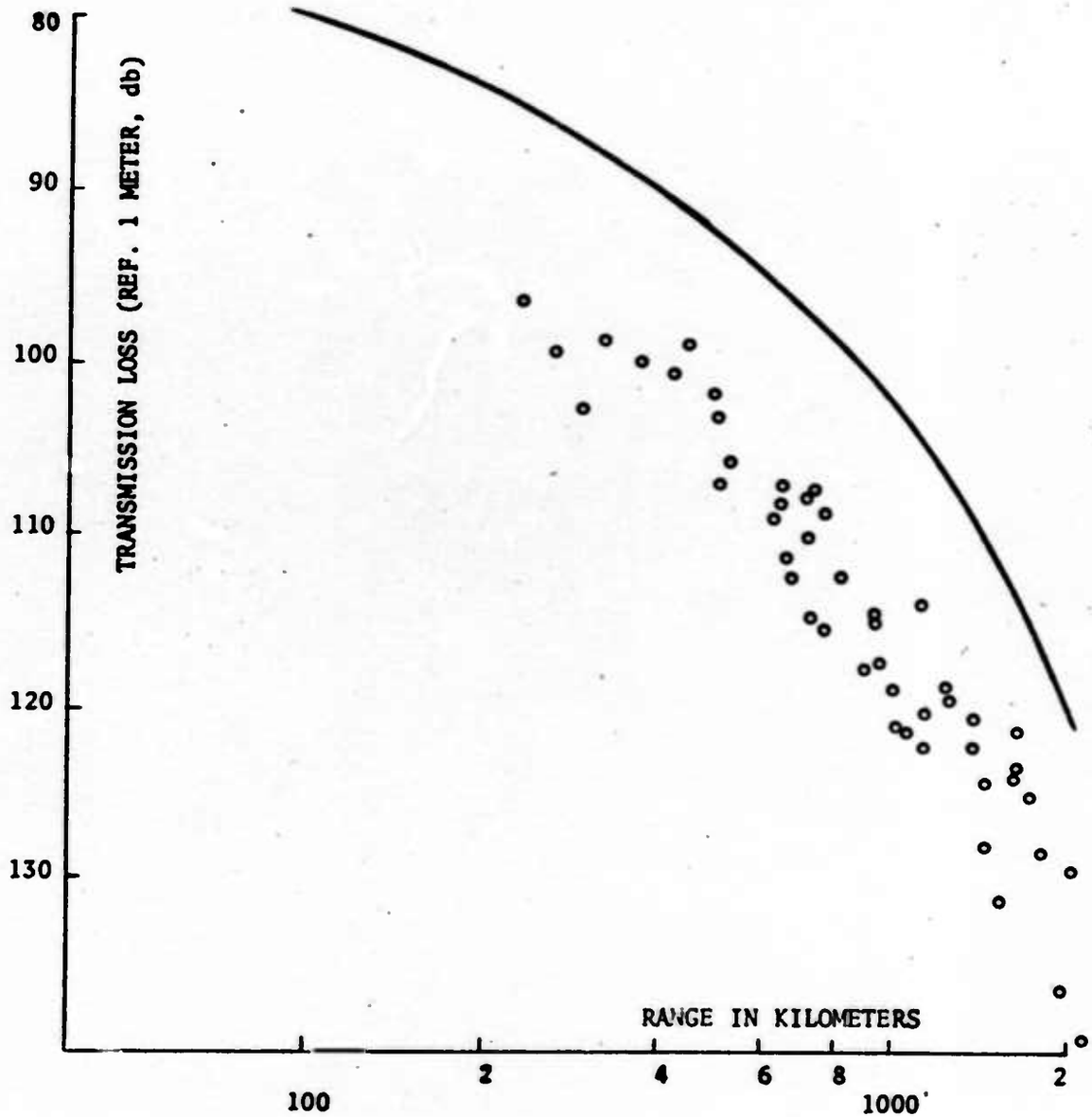

CALCULATED RESULTS AND BEST FIT CURVE FROM MEASUREMENTS (B. M. BUCK)

GROUP II o DEPTH OF SOURCES = 210 FT., DEPTH OF RECEIVERS = 200 FT.

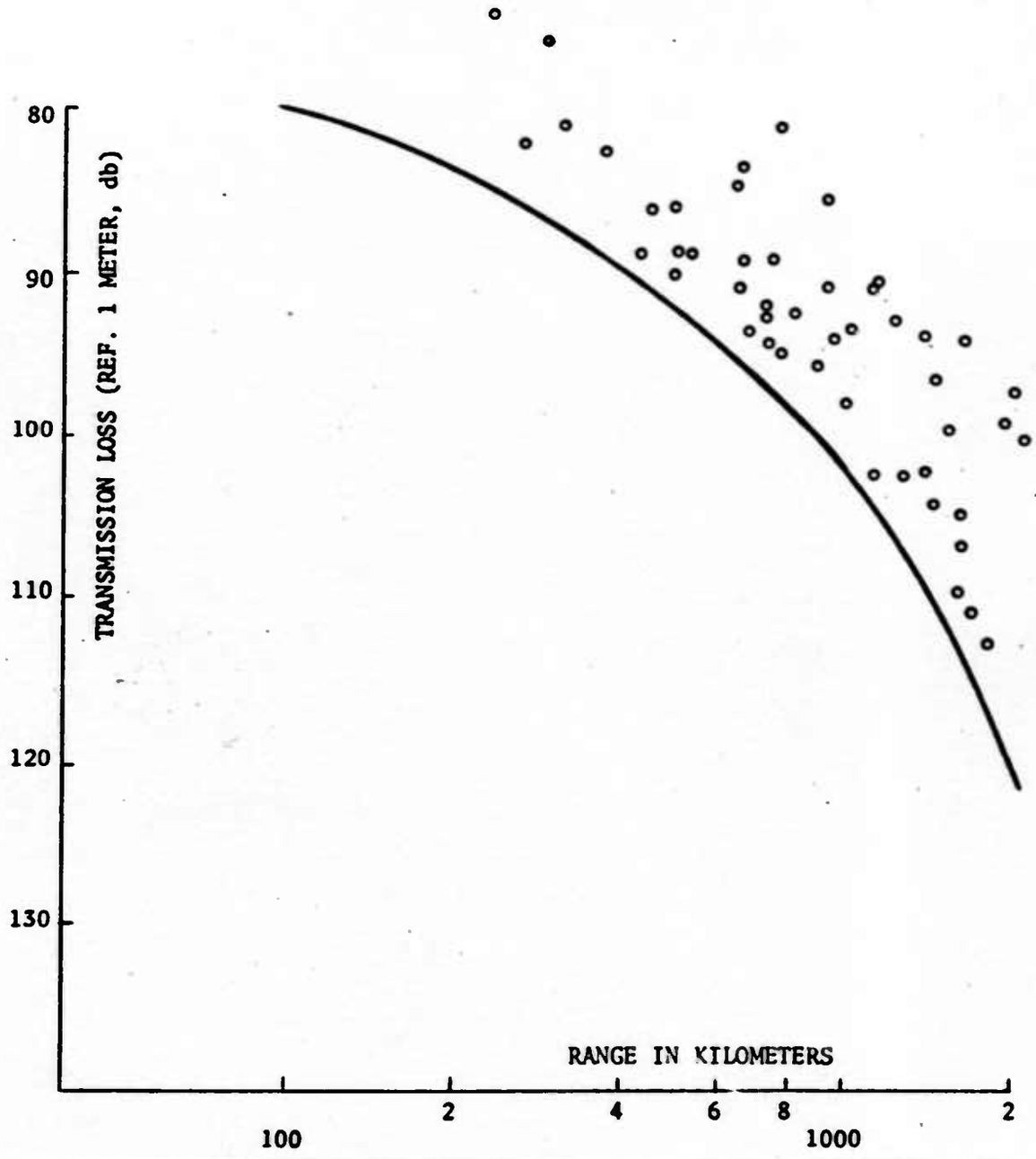

CALCULATED RESULTS AND BEST FIT CURVE FROM MEASUREMENTS (B. M. BUCK)

GROUP II o DEPTH OF SOURCES = 410 FT., DEPTH OF RECEIVERS = 200 FT.

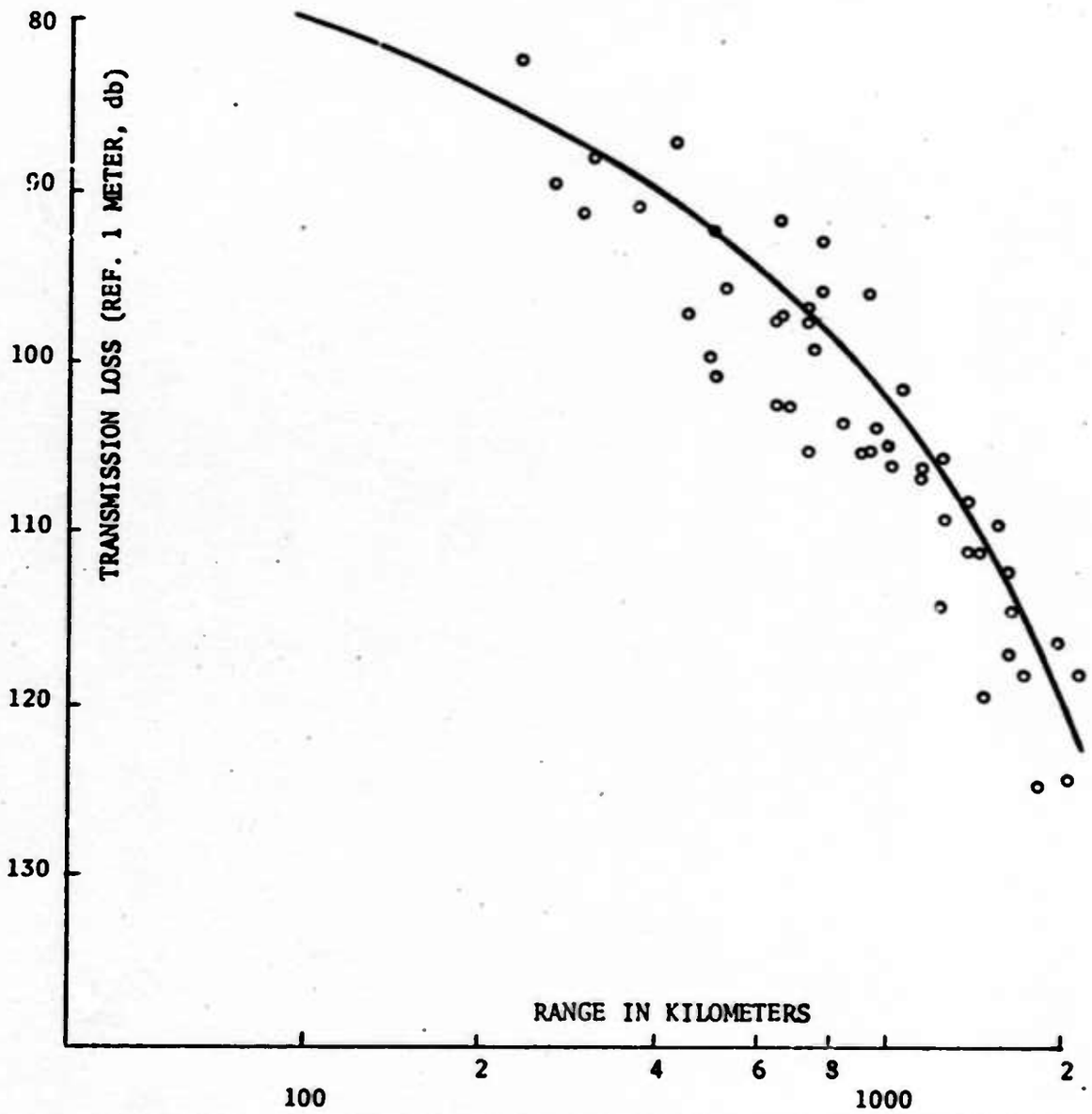

CALCULATED RESULTS AND BEST FIT CURVE FROM MEASUREMENTS (B. M. BUCK)

GROUP II • DEPTH OF SOURCES = 610 FT., DEPTH OF RECEIVERS = 200 FT.

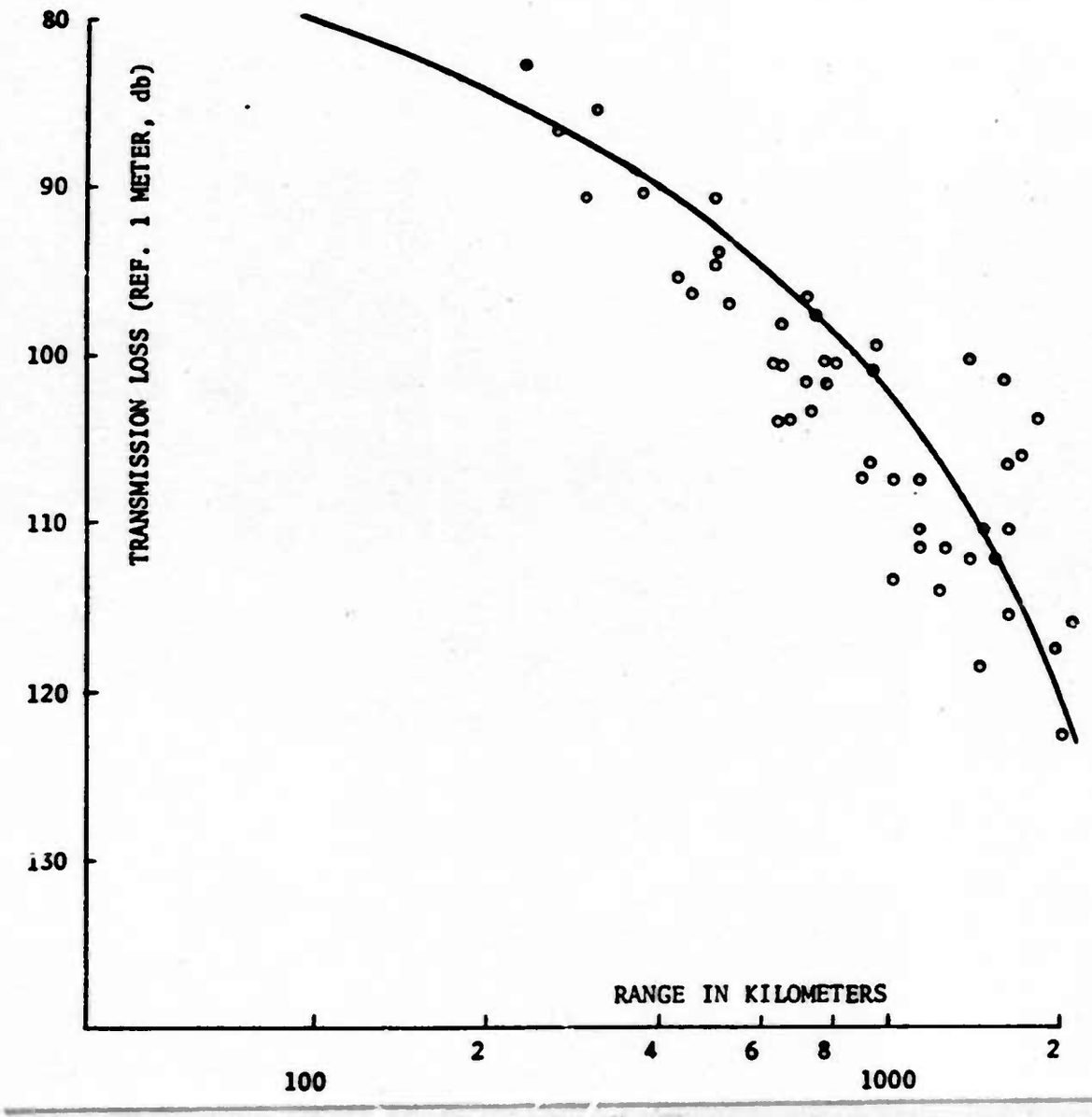

CALCULATED RESUI ..D BEST FIT CURVE FROM MEASUREMENTS (B. M. BUCK)

GROUP III ○
GROUP IV □ DEPTH OF SOURCES = 20 FT., DEPTH OF RECEIVERS = 200 FT.
GROUP V △

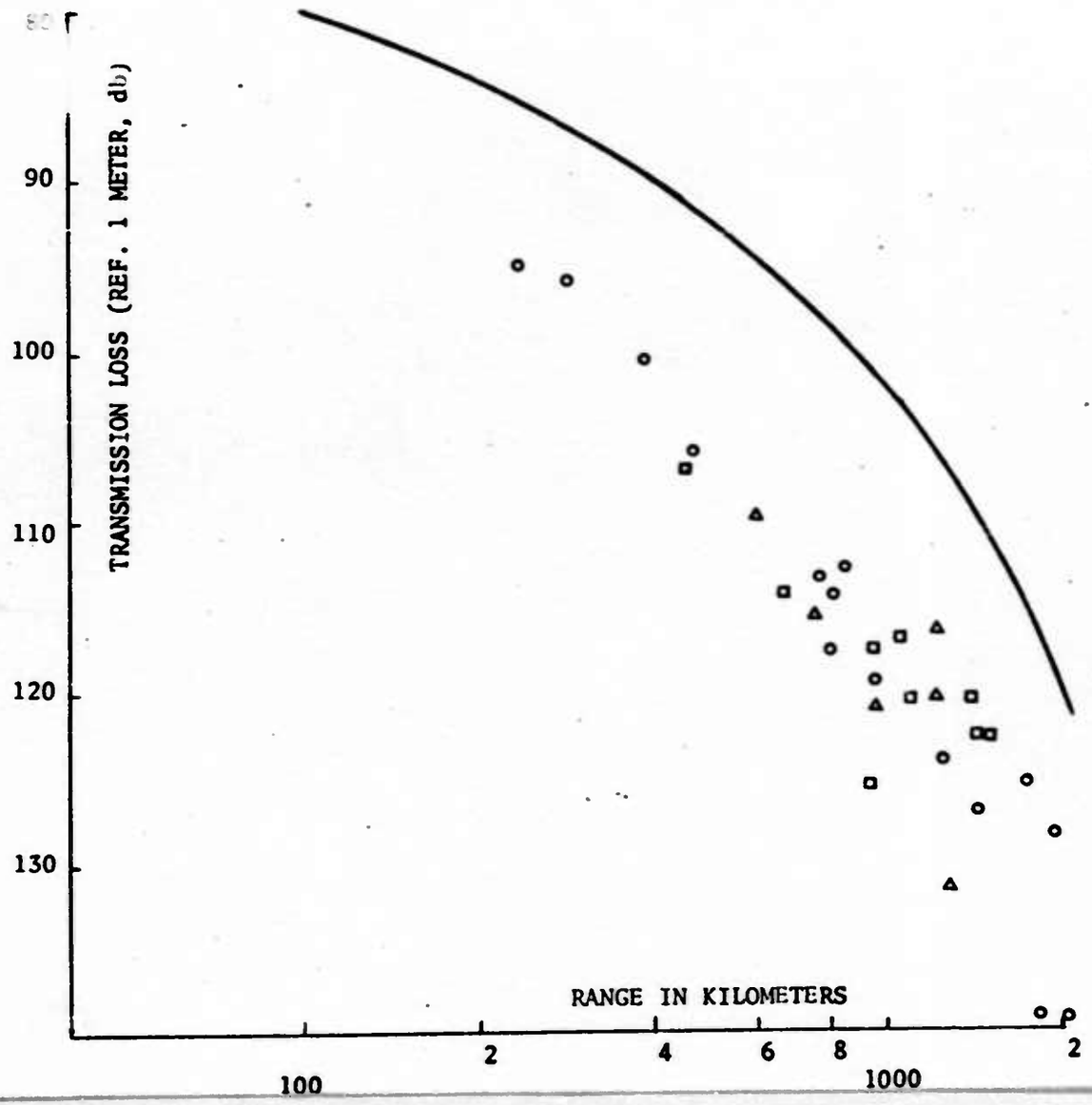

CALCULATED RESULTS AND BEST FIT CURVE FROM MEASUREMENTS (B. M. BUCK)

GROUP III ○
GROUP IV □ DEPTH OF SOURCES = 210 FT., DEPTH OF RECEIVERS = 200 FT.
GROUP V △

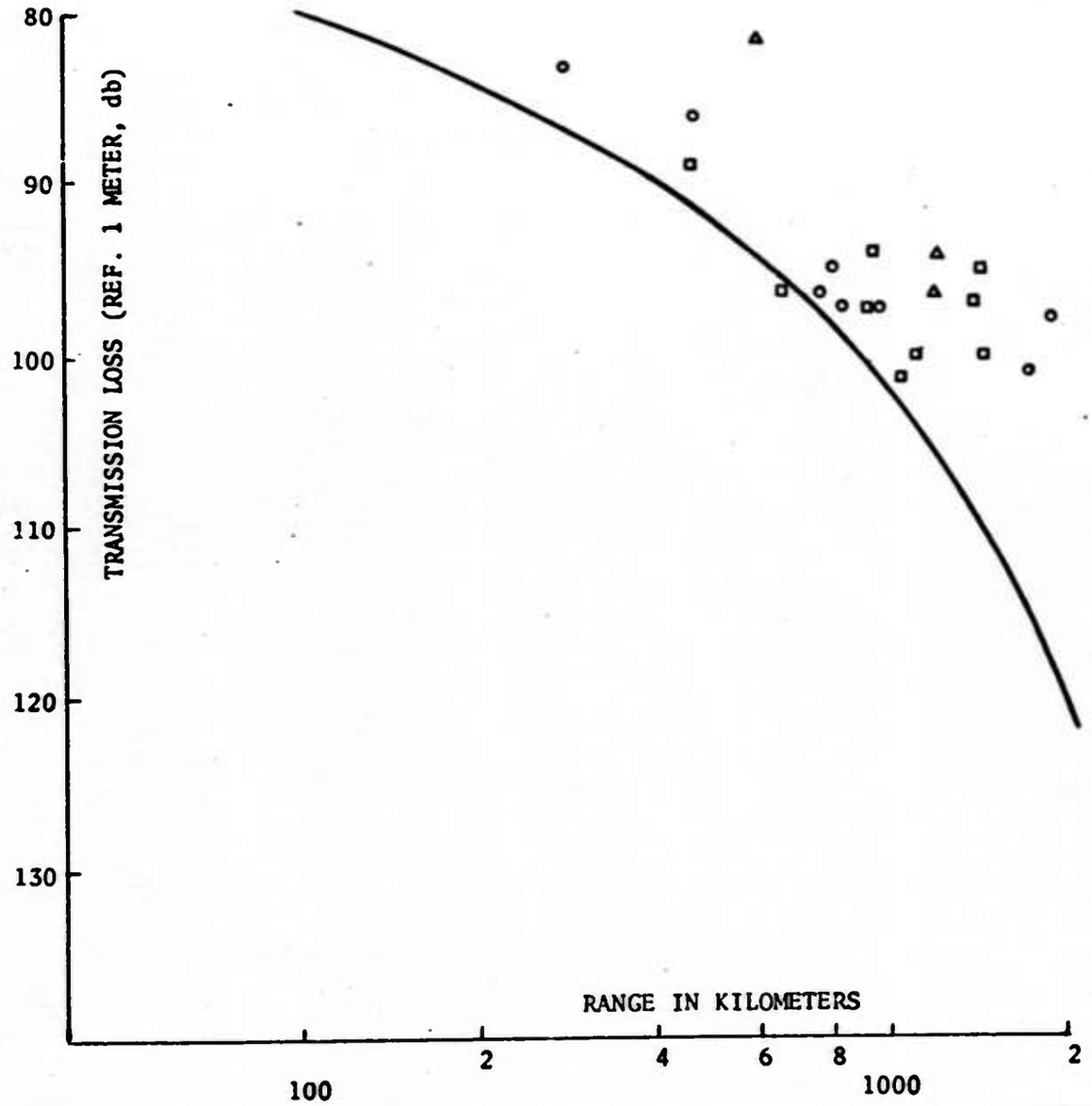

CALCULATED RESULTS AND BEST FIT CURVE FROM MEASUREMENTS (B. M. BUCK)

GROUP III ○
GROUP IV □ DEPTH OF SOURCES = 410 FT., DEPTH OF RECEIVERS = 200 FT.
GROUP V △

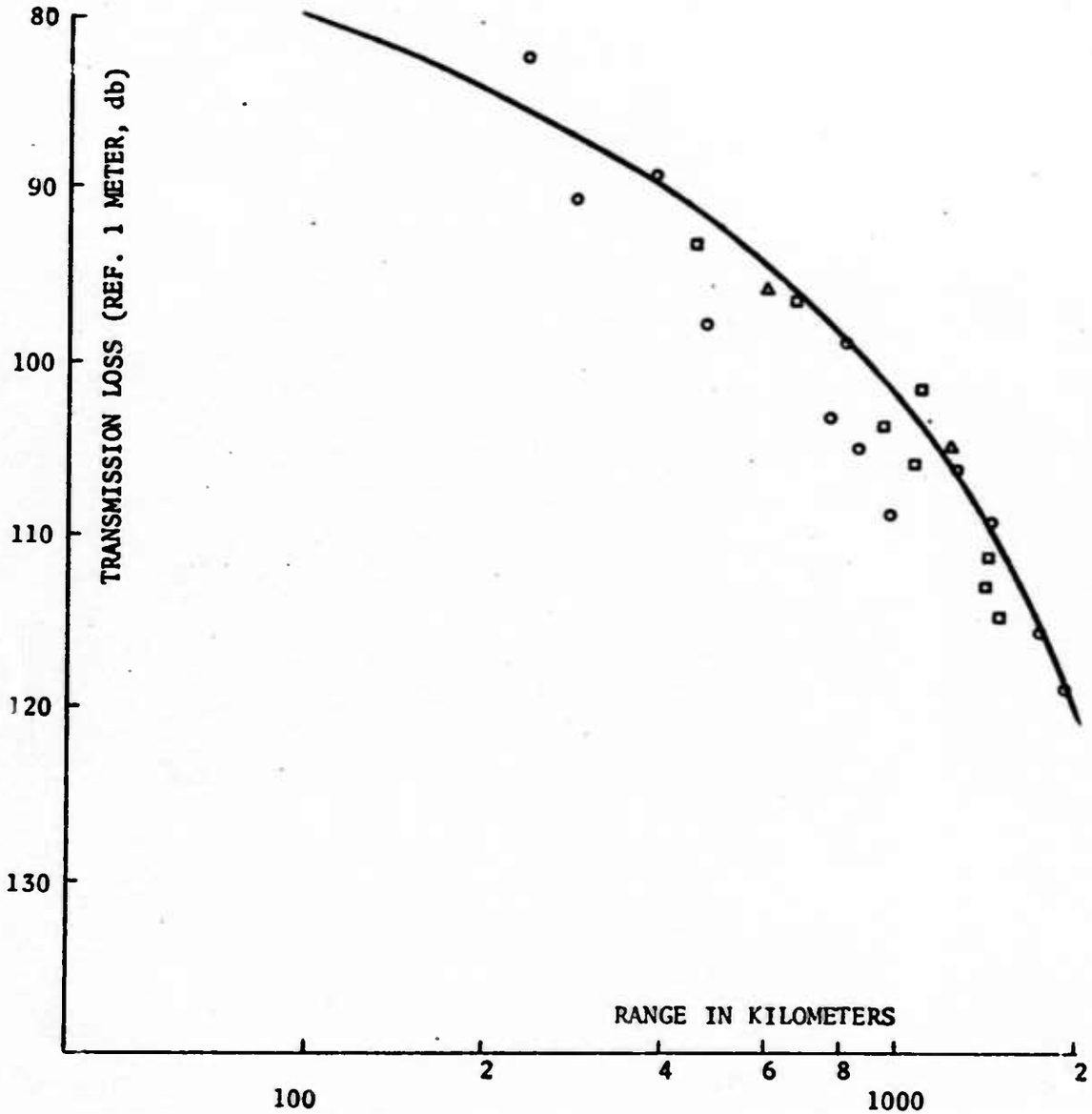

CALCULATED RESULTS AND BEST FIT CURVE FROM MEASUREMENTS (B. M. BUCK)

GROUP III ○
GROUP IV □ DEPTH OF SOURCES = 610 FT., DEPTH OF RECEIVERS = 200 FT.
GROUP V ▲

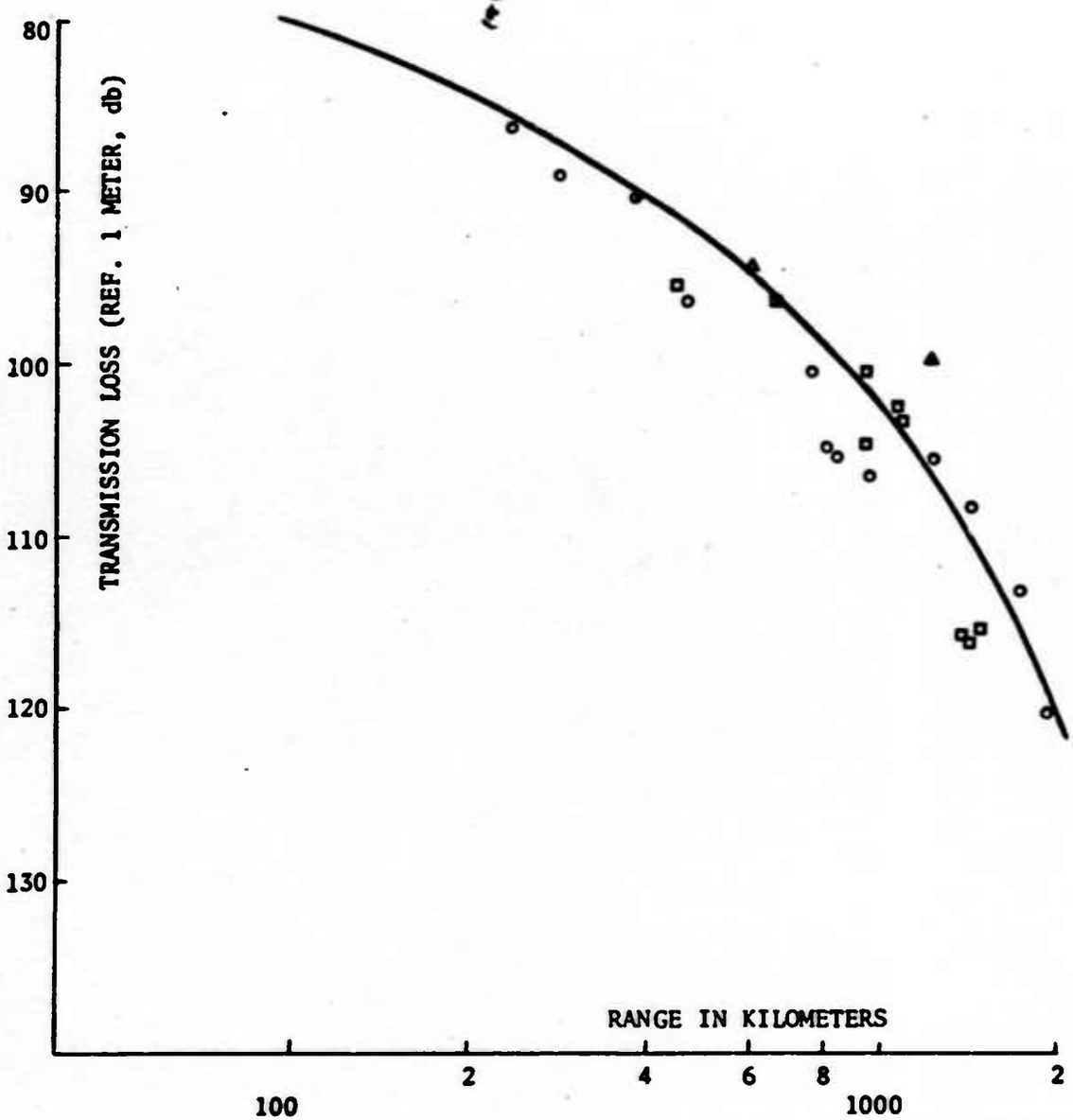

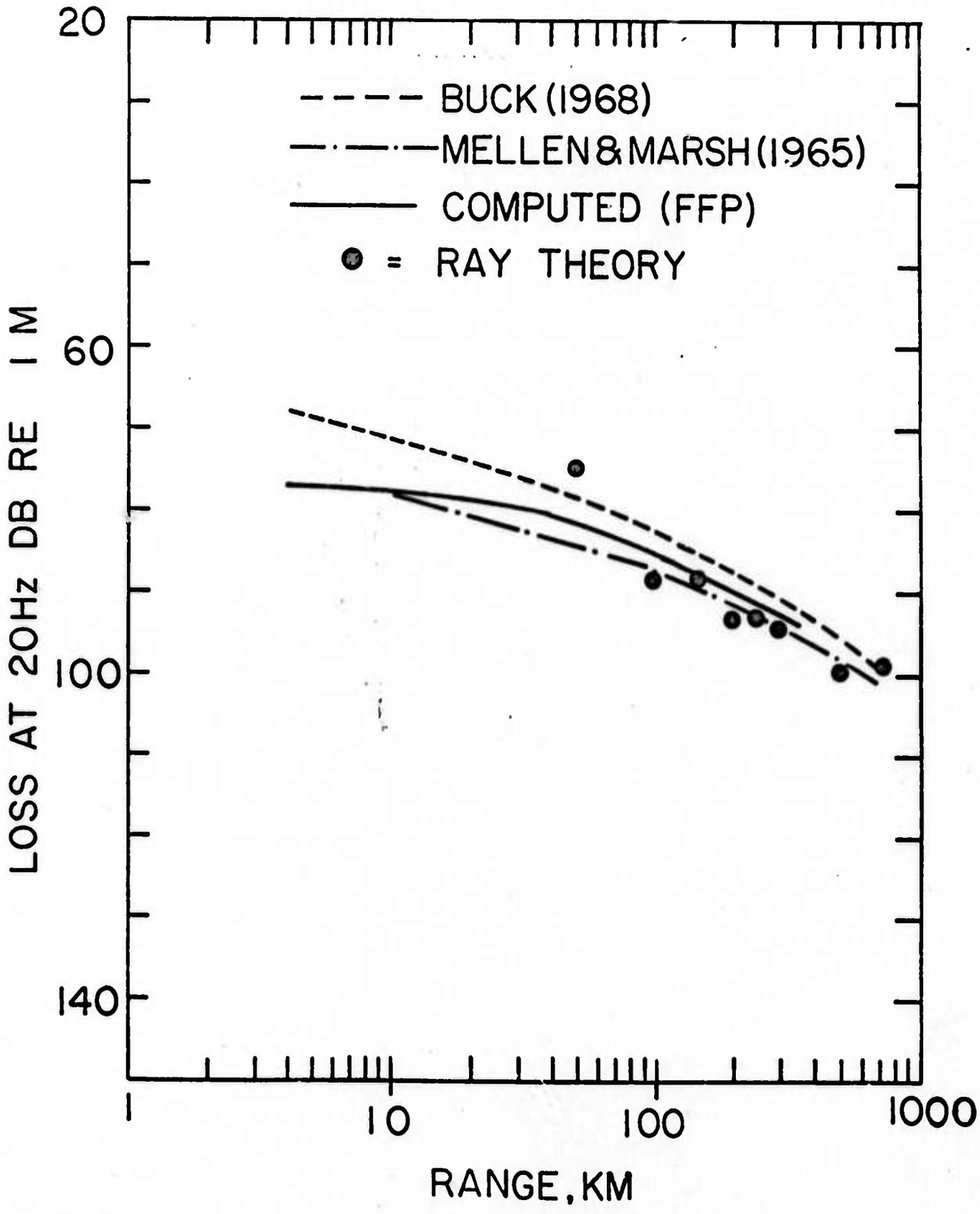
20
60
100
140
LOSS AT 20Hz DB RE 1 M
BUCK (1968)
MELLEN & MARSH (1965)
COMPUTED (FFP)
= RAY THEORY
1
10
100
1000
RANGE, KM

ACKNOWLEDGMENT

Professors C. E. Pearson and Y. Vagners, both of the University of Washington and consultant to the present study, are contributors of Section 2 and 3 of this report respectively. I am thankful for their participation and fruitful discussions.

The joint work with Lamont-Doherty Geological Observatory has been a very happy and satisfying experience. Dr. H. Kutschale visited Aerophysics Research Corporation at Bellevue several times and has provided many valuable and helpful suggestions.

I also like to thank the entire staff of Aerophysics Research Corporation for their interest and programming support, in particular, for the use of contour plot subroutines written by Mr. D. S. Hague, president of the Company.